Cell Biomaterials

Article

A neurodevelopment-inspired self-evolving scaffold for nerve regeneration

Graphical abstract

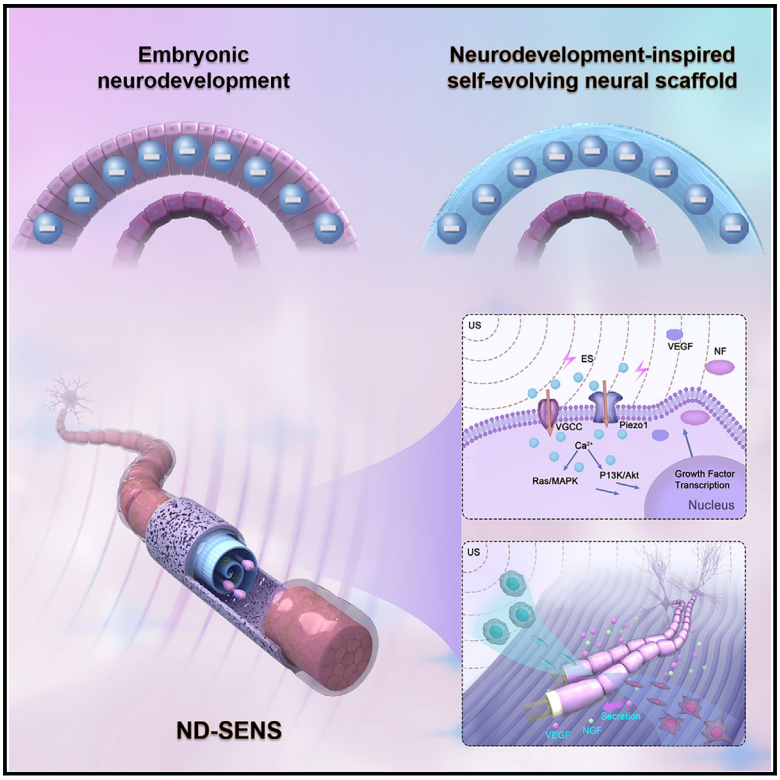

Highlights

- A biohybrid neural scaffold inspired by embryonic structure (ND-SENS) was proposed
- ND-SENS mimicked the physical and chemical signals of embryonic neural development
- ND-SENS promoted the recruitment and differentiation of endogenous stem cells
- ND-SENS achieved sciatic nerve repair comparable to autologous transplantation

Authors

Yizhu Shan, Lingling Xu, Xi Cui, ..., Kailiang Ren, Dan Luo, Zhou Li

Correspondence

luodan@binn.cas.cn (D.L.), zli@binn.cas.cn (Z.L.)

In brief

Inspired by embryogenesis, we developed a biohybrid neurodevelopment-inspired self-evolving neural scaffold (ND-SENS), which successfully simulated the electrical environment and paracrine signals during embryonic development, thereby promoting the recruitment and differentiation of endogenous stem cells, ultimately achieving efficient repair of peripheral nerve injuries comparable to autologous transplantation.

Shan et al., 2025, Cell Biomaterials *1*, 100006
February 25, 2025
https://doi.org/10.1016/j.celbio.2024.100006

CellPress

Please cite this article in press as: Shan et al., A neurodevelopment-inspired self-evolving scaffold for nerve regeneration, Cell Biomaterials (2024), https://doi.org/10.1016/j.celbio.2024.100006

Cell Biomaterials

CellPress
OPEN ACCESS

Article

A neurodevelopment-inspired self-evolving scaffold for nerve regeneration

Yizhu Shan,[1,3,8] Lingling Xu,[1,4,8] Xi Cui,[1,3,8] Jinxi Zhang,[1] Han Ouyang,[3] Xiangxiang Wang,[1,3] Jing Huang,[1,3] Jiangtao Xue,[5] Kefei Wang,[6] Dongchuan Wang,[1,7] Engui Wang,[1] Kailiang Ren,[1,3] Dan Luo,[1,3,*] and Zhou Li[1,2,3,9,*]

[1]Beijing Institute of Nanoenergy and Nanosystems, Chinese Academy of Sciences, Beijing 100083, China
[2]Tsinghua Changgung Hospital, School of Clinical Medicine, School of Biomedical Engineering, Tsinghua Medicine, Tsinghua University, Beijing 100084, China
[3]School of Nanoscience and Engineering, University of Chinese Academy of Sciences, Beijing 100049, China
[4]CAS Key Laboratory for Biomedical Effects of Nanomaterials and Nanosafety and CAS Center for Excellence in Nanoscience, National Center for Nanoscience and Technology, Beijing 100190, China
[5]School of Medical Technology, Beijing Institute of Technology, Beijing 100081, China
[6]Department of Mathematics and Statistics, McGill University, Montreal, QC H3A0G4, Canada
[7]International Division, the Second High School Attached to Beijing Normal University, Beijing 100192, China
[8]These authors contributed equally
[9]Lead contact
*Correspondence: luodan@binn.cas.cn (D.L.), zli@binn.cas.cn (Z.L.)
https://doi.org/10.1016/j.celbio.2024.100006

THE BIGGER PICTURE Peripheral nerve injury can cause a series of pathological changes, and autologous nerve grafting, as the current gold standard of clinical treatment, is limited by the risk of surgical complications and the accessibility of donor sources. Although the repair capacity of nerve damage in adulthood becomes very limited, the growth and development of neural tissue is rapid and programmed during embryonic development. Inspired by the embryonic neural development process, we developed a biohybrid neurodevelopment-inspired self-evolving neural scaffold (ND-SENS), which consisted of piezoelectric film with ordered micro-nano structures, extracellular matrix-like hydrogel, and stem cells, and was further rolled into an embryo-like cylindrical shape. The biohybrid ND-SENS mimicked the physical and chemical signals generated by embryonic development. ND-SENS constructed an embryogenesis-like endogenous electrical environment to promote the differentiation of loaded mesenchymal stem cells; meanwhile, the differentiated stem cells in ND-SENS simulated the chemical environment of embryonic development through paracrine secretion, which further induced the recruitment and differentiation of endogenous stem cells, ultimately achieving self-evolving axon outgrowth. ND-SENS showed excellent neurorestorative effects in both dorsal root ganglion explant growth model and rat sciatic nerve injury model. After ND-NENS treatment, the regenerated nerve tissue had no significant difference from autologous transplantation in terms of the expression of mature neuron markers and myelin thickness; rats treated with ND-SENS could significantly improve their muscle atrophy and restore their motor ability. This work confirms that scaffold design inspired by embryonic development can effectively enhance the regenerative capacity of defective tissues, bringing new ideas for future tissue engineering research.

SUMMARY

Inspired by the embryonic neural development process, we proposed a biohybrid neurodevelopment-inspired self-evolving neural scaffold (ND-SENS), which consisted of piezoelectric film with ordered micro-nano structures, extracellular matrix-like hydrogel, and stem cells. ND-SENS constructed an embryogenesis-like endogenous electrical environment to promote the differentiation of loaded mesenchymal stem cells; meanwhile, the differentiated stem cells in ND-SENS simulated the chemical environment of embryonic development through paracrine secretion, which further induced the recruitment and differentiation of endogenous stem cells, ultimately achieving self-evolving axon outgrowth. ND-SENS showed excellent neurorestorative effects in both dorsal root ganglion explant growth model and rat sciatic nerve injury model. After ND-NENS treatment, the proportion of mature neuron marker-positive area (77.39% ± 1.71%) and myelin sheath thickness

Please cite this article in press as: Shan et al., A neurodevelopment-inspired self-evolving scaffold for nerve regeneration, Cell Biomaterials (2024), https://doi.org/10.1016/j.celbio.2024.100006

CellPress
OPEN ACCESS

Cell Biomaterials
Article

(0.71 ± 0.07 μm) of regenerated nerve tissue were not significantly different from those of autologous transplantation. This biomimetic scaffold design inspired by embryonic development will bring new ideas to tissue engineering.

INTRODUCTION

Peripheral nerve injury (PNI), which is usually caused by trauma, mechanical compression, metabolic disorders, inflammation, or infection, can lead to severe disability, inflict immense psychological harm to patients, and also impose a heavy burden on families and society.[1] PNI triggers a series of pathological changes in nerves and the surrounding tissues, including axonal rupture, the interruption of electrical signal transmission by nerves, the atrophy of innervated muscles, disrupting homeostasis of the microenvironment homeostasis at the injured site and making the nerve repair process difficult.[2,3] To date, the gold standard treatment for PNI is autogenous nerve transplantation.[4] However, to obtain autologous nerves, additional surgical interception of a normal peripheral nerve is needed, increasing surgical difficulty and the risk of surgical complications at the donor site. In addition, the sources of donor nerves are limited, and obtaining nerves with a diameter and length consistent with those of the damaged nerve at the patient's injury site is difficult.[5] Therefore, developing alternative strategies to recreate the neural-like microenvironment and ultimately achieve therapeutic effects matching those of autologous transplantation is highly important.

Nerve regeneration strategies based on the combination of tissue engineering scaffolds with stem cells are potential methods for treating PNI.[6,7] Conventional neural scaffolds are primarily utilized to facilitate nerve regeneration in damaged areas by constructing biomimetic structures of nerve fibers. However, morphology-based biomimetic scaffolds usually have limitations such as singular functionality and inadequate bioactivity, making it challenging to create a microenvironment conducive to tissue regeneration or to effectively induce endogenous stem cell homing. The incorporation of cytokines into neural scaffolds has been shown to significantly enhance their bioactivity and improve tissue repair in the short term. Nevertheless, the long-term efficacy of these composite scaffolds remains uncertain due to constraints related to the amount of loaded cytokines, the release kinetics of the cytokines, and their degradation within the *in vivo* environment. Furthermore, tissue regeneration is a highly complex, multi-phase process; and the delivery of only one or a few cytokines may not be sufficient to support each stage of neural repair. The development of a new generation of neural scaffolds can be inspired by the physiological regeneration and developmental processes of tissues. However, with the growth and development of the human body, neurogenesis decreases, and the renewal and repair capacity of the nervous system in adulthood is very limited.[8,9] Although nerve damage repair can be accelerated by connecting nerve conduits, it is still difficult to achieve a therapeutic effect comparable to those of autologous nerve transplantation.[10] Interestingly, during embryonic development, the growth and development of neural tissue are rapid and programmed, in a process known as embryonic induction, a specific group of cells influence neighboring cells and determine their differentiation direction over time.[11–13] Primary embryonic induction refers to a phenomenon in which the notochord mesoderm induces the neuroectoderm above it to develop into the nervous system. First, induced by the notochord, which acts as an organizer, the ectoderm gradually thickens and forms a neural plate. Central depression of the neural plate subsequently forms the neural groove, which closes to form the neural tube. The neural tube then detaches from the primitive ectoderm and is covered by the surface ectoderm. The neuroepithelial cells constituting the wall of the nerve tube continue to proliferate, migrate, and differentiate to form neuroblasts and glioblasts.[14–16] Throughout embryonic development, embryogenesis is regulated by two types of signals: physical stimulation mediated by endogenous electric fields[17] and paracrine and juxtacrine signals from neighboring cells.[18] The cellular uptake of Na ions from the environment leads to the generation of ion currents and potential differences, and a potential difference between different regions creates an intraembryonic voltage gradient, giving rise to endogenous electric fields.[19–21] During the entire neural development process, the proliferation, migration, and differentiation of neuroepithelial cells depend on electrical activity to varying degrees.[22] In addition, under the promotion of electrical activity, the paracrine secretion of some neurotrophic factors can also promote the differentiation of the ectoderm to form the nervous system.[23] The microenvironment formed by electrical signals and secreted chemical signals in which embryonic development occurs is the key to achieving epigenetic regulation and promoting neural development.

Inspired by the process of embryonic neural development, we developed a biohybrid self-evolving tissue engineering scaffold that successfully simulates the electrical environment and paracrine signals during embryogenesis to promote the recruitment and differentiation of endogenous stem cells, thereby achieving efficient repair of peripheral nerve damage. Different from the traditional morphologically induced neural scaffold, the neurodevelopment-inspired self-evolving neural scaffold (ND-SENS) proposed in this study successfully promoted the recruitment and differentiation of endogenous stem cells by simulating the complex physical and chemical microenvironment during embryonic induction, thereby achieving effective repair of peripheral nerve damage. In ND-SENS, mesenchymal stem cells (MSCs) are first loaded onto a membrane composed of piezoelectric poly-L-lactic acid (PLLA) fibers, and upon further addition of a hydrogel that mimics the extracellular matrix (ECM), the membrane is then curled into a three-dimensional tubular structure, simulating formation of the neural tube by neuroepithelial cells (Figure 1A). This ND-SENS provides physical and chemical signals similar to those of the embryonic induction process: the electric field formed by the piezoelectric potential on the surface of the PLLA membrane under ultrasound-induced excitation simulates the endogenous electrical environment during embryonic development; furthermore electrical stimulation

Please cite this article in press as: Shan et al., A neurodevelopment-inspired self-evolving scaffold for nerve regeneration, Cell Biomaterials (2024), https://doi.org/10.1016/j.celbio.2024.100006

promotes the differentiation of MSCs and enhances their paracrine effects, which further induces the recruitment and differentiation of endogenous stem cells, ultimately promoting axonal growth (Figure 1B). The ND-SENS showed excellent nerve repair effects in both an *in vitro* dorsal root ganglion (DRG) explant model and an *in vivo* rat sciatic nerve injury model. The sciatic nerves of rats treated with ND-SENS exhibited good repair effects in terms of histology and function. This biomimetic scaffold design inspired by embryonic development will lead to new ideas in the field of tissue engineering.

RESULTS AND DISCUSSION

Controllable fabrication of ordered micro/nanostructured piezoelectric membranes that mimic the morphology of the ectoderm and intraembryonic potential differences

The ND-SENS is a biohybrid smart material constructed by integrating living cells into electroactive materials. Among these materials, the selection of electroactive materials is the key to successfully constructing the ND-SENS and simulating the embryonic microenvironment. Achieving this microenvironment requires not only the rapid construction of a controllable electrical gradient similar to the transembryonic potential difference but also sufficient support for living cells and material biosafety that meets requirements for translational medicine. Poly-L-lactic acid (PLLA), as an organic material with good biocompatibility and degradability, has been widely used in drug carriers and tissue engineering scaffolds. More importantly, PLLA has unique piezoelectric properties that are different from those of traditional piezoelectric materials such as lead zirconate titanate (PZT) and polyvinylidene fluoride (PVDF).[24] Polarization is not required to induce the piezoelectric properties of the entirety of PLLA material. Instead, piezoelectric properties in the shear direction (d_{14}) are achieved through stretching or electrospinning to obtain molecular chains that are arranged in a consistent direction. Specifically, when the PLLA molecular chain is subjected to shear strain, the dipole of the carbonyl bond rotates, resulting in a polarity change perpendicular to the shear plane.[25,26] In our system, we obtained a membrane structure composed of unidirectionally aligned PLLA fibers through a modified electrospinning strategy. To control the fiber membrane to adapt to the damaged neural tissue in terms of scale and provide an ordered surface micro/nanostructure suitable for regulating the directional growth of cells, different electrospinning parameters, including the solution concentration, receiving distance, and rotation speed, were systematically explored (Figure S1). Finally, a PLLA membrane composed of order-arranged fibers with a diameter of approximately 1 μm was obtained. Fourier transform infrared (FTIR) spectroscopy demonstrated that electrospinning transformed the orientation of PLLA molecular chains from a disordered phase to an ordered phase (Figure S2). The orientation of the molecular main chains was consistent with the direction of fiber extension, so the carbonyl bonds also exhibited the same arrangement angle, as shown in the schematic diagram of Figure 2A.[27]

Annealing temperatures can significantly affect the crystallinity and crystal phase of PLLA polymers, which directly affect the piezoelectric properties of the material.[28] Since the melting temperature of PLLA is approximately 169°C, we selected three gradient annealing temperatures (115°C, 135°C, and 155°C) below the melting point as the experimental conditions and analyzed the crystallization performance of the PLLA fiber membranes at these different annealing temperatures by X-ray diffraction (XRD) and differential scanning calorimetry (DSC). Figure 2B shows that the PLLA piezoelectric film possessed an extremely strong diffraction peak near 16.9°, corresponding to the (200)/(110) crystal face of the PLLA standard card (00-054-1917), representing the α crystalline phase, and a small diffraction peak corresponding to the (230) crystal face, corresponding to the α′ crystalline phase, at 19.1°. The results show that the crystallinity of PLLA was improved after annealing, and most of PLLA was converted into α-crystalline phase. As the annealing temperature increased, the (200)/(110) crystallization peak gradually shifted in the high angle direction. This is because the α′ crystalline phase of PLLA presents a disordered and loosely packed crystal structure related to the loose helical chain packing. When the annealing temperature increased, PLLA transformed from the α′ phase to the α phase, and the helical chain packing of the molecular chains in the unit cell became more compact and ordered.[29] The compact molecular chain arrangement leaded to a decrease in the lattice spacing d(200)/(110) and d(203), so the position of the crystal diffraction peak shifted to a higher-angle direction according to the Bragg equation. DSC revealed that the glass transition temperature of the unannealed PLLA film was 53°C and that the crystallization temperature was 85°C (representing the crystallization enthalpy, ΔH_c). In comparison, the annealed PLLA film exhibited only a melting enthalpy peak (ΔH_m), indicating that the annealing treatment caused glass transition and crystallization of the piezoelectric polymer (Figure 2C). The crystallinity of a fiber membrane can be calculated using the following formula[30]:

$$x = 100\% \times \left(\frac{\Delta Hm - \Delta Hc}{93.6 \mathrm{J} \cdot g^{-1}} \right)$$

In this formula, 93.6 $J \cdot g^{-1}$ represents the percentage of PLLA at 100% crystallization (ΔH_f). The calculation further confirmed that with increasing annealing temperature, the crystallinity of the PLLA film gradually increased (the crystallinity was 55% at 135°C and 62% at 155°C, as shown in Table S1). In addition, the piezoelectric coefficient of the prepared PLLA film was tested using a custom d_{14} measuring device (Figure S3A) and calculated using the following formula[31,32]:

$$d_{14} = \frac{\rho_{sur}}{\sigma_{14}} = \frac{Q_{sur}}{S_{sur}} \left(\frac{F}{S_{cro}} \right)^{-1} = \frac{S_{cro}}{S_{sur}} \cdot \frac{\int Idt}{F}$$

where ρ_{sur} is the surface charge density, σ_{14} represents the tensile cross-sectional stress, Q_{sur} represents the amount of surface charge, S_{sur} represents the surface area where the charge is generated, F represents the corresponding tensile force, S_{cro} represents the tensile cross-sectional area, and I is the current.

The piezoelectric coefficients of the PLLA films prepared at three different annealing temperatures (115°C, 135°C, and

Please cite this article in press as: Shan et al., A neurodevelopment-inspired self-evolving scaffold for nerve regeneration, Cell Biomaterials (2024), https://doi.org/10.1016/j.celbio.2024.100006

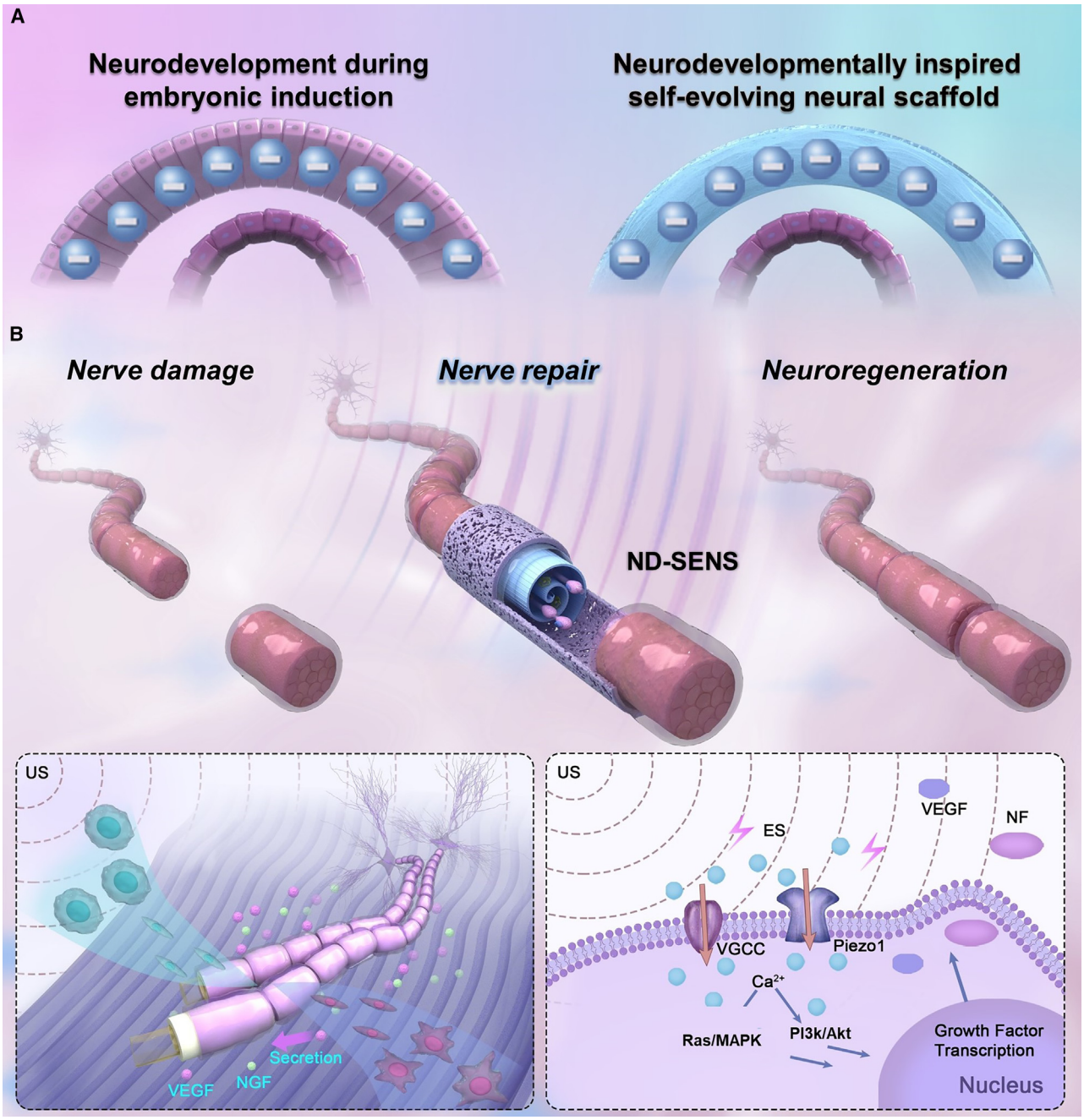

Figure 1. Schematic diagram of the biohybrid ND-SENS

(A) Schematic diagram showing cross-section of the early embryo and ND-SENS.

(B) The ND-SENS simulates intraembryonic endogenous electric fields to promote stem cell differentiation and increase paracrine signaling to induce endogenous stem cell recruitment.

155°C) were 5.95, 7.73, and 8.91 pC/N, respectively, indicating that the annealing temperature was positively correlated with the piezoelectric coefficient (Figures 2D and S3B). We also measured the piezoelectric coefficient of racemic polylactic acid (PLA) films prepared via the same electrospinning method, and the results revealed that only the PLLA fibers exhibited certain piezoelectric properties (Figure S3C). Therefore, the PLLA fiber membrane annealed at 155°C with high piezoelectric coefficients was used in subsequent experiments, whereas non-piezoelectric PLA with similar chemical composition and micro-nanostructure was used as the control group.

During embryonic development, along with the germ layer differentiation, the embryo gradually adopts a cylindrical structure, and an annular intraembryonic potential difference on the curved

Please cite this article in press as: Shan et al., A neurodevelopment-inspired self-evolving scaffold for nerve regeneration, Cell Biomaterials (2024), https://doi.org/10.1016/j.celbio.2024.100006

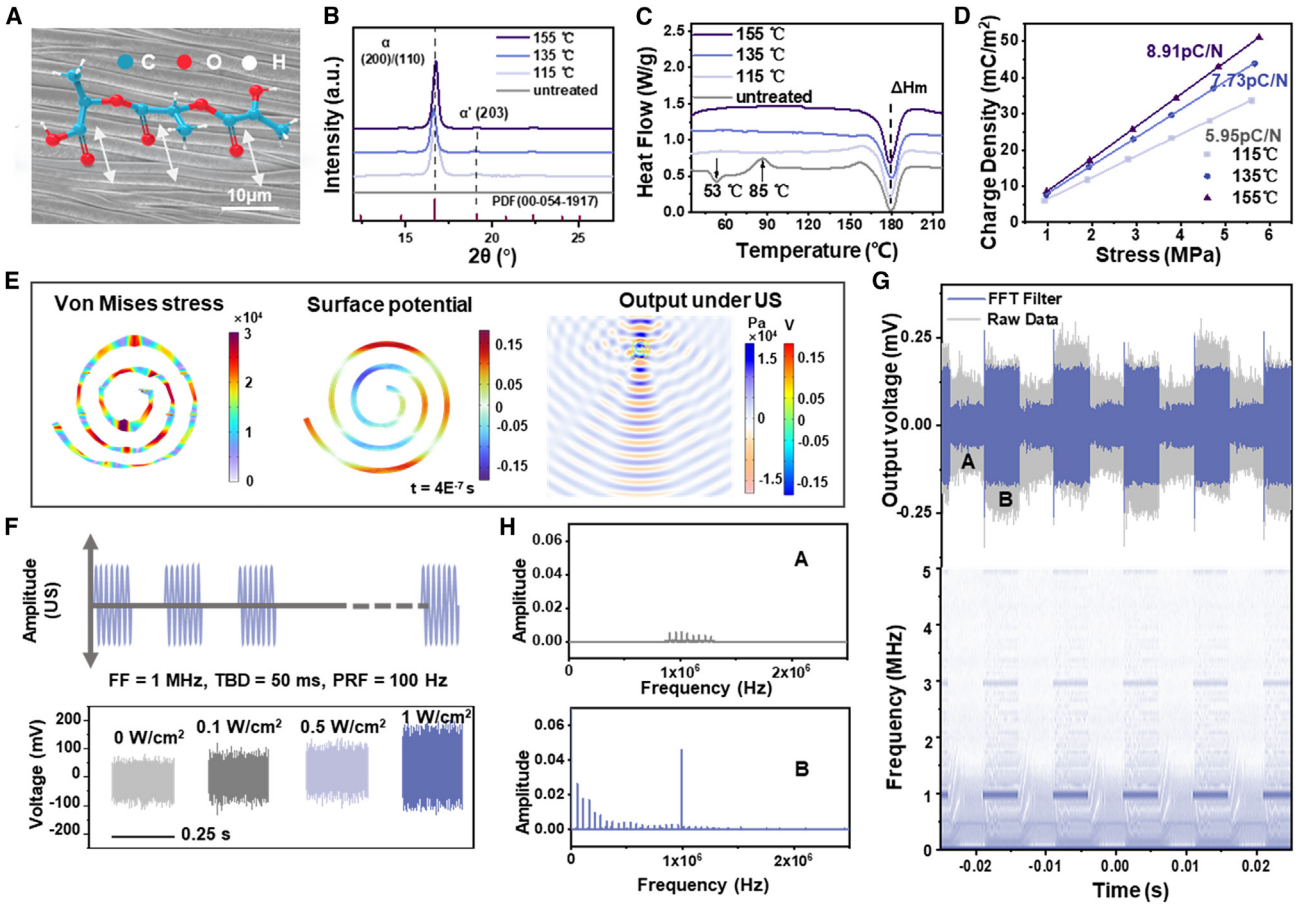

Figure 2. Structural and electrical properties of the piezoelectric membrane in the ND-SENS

(A) Microstructure of PLLA and the schematic diagram of the internal molecular structure of PLLA.
(B) XRD characterization data of PLLA films at different annealing temperatures.
(C) DSC characterization data of PLLA films at different annealing temperatures.
(D) Output charge as a function of applied stress for the PLLA films at different annealing temperatures.
(E) Simulation of the stress and surface potential generated by the PLLA film under curling conditions in an ultrasonic field.
(F) Schematic diagram of the ultrasonic waveform and voltage output by the PLLA membrane under different ultrasonic intensities.
(G) Voltage output signals at 0.5 W/cm^2 (top) and the fast Fourier tranfer (FFT)-filtered signal, as well as the results of corresponding spectral analysis (bottom).
(H) Fourier transform spectrum analysis of signals in regions of (A) and (B) in (G).

surface is generated. Since the prepared PLLA fiber membrane was flexible, it could be rolled into a cylinder that simulates in shape of the ectoderm. To confirm whether the PLLA fiber membrane could also simulate the electrical properties of the ectoderm and achieve distribution of the electric potential on the three-dimensional curved surface, we quantified the piezoelectric output of the three-dimensional curled PLLA fiber membranes through theoretical calculations and experiments. COMSOL simulation revealed the strain and corresponding surface potential of the curled cylindrical PLLA membrane under 1.0 MHz with 1.0 W/cm^2 ultrasonic stimulation (US), and electric field changes in the US field (Figures 2E and S4). The results indicated that with the application of ultrasound, the PLLA film exhibited a certain degree of vibration, resulting in potential changes. The actual electrical output of the curled cylindrical PLLA membrane under US at different intensities was then tested experimentally (Figure S5). As the intensity of the US increased, the electrical output of the curled PLLA gradually increased. The piezoelectric voltage generated by the cylindrical PLLA membrane reached ~0.22 V when the applied ultrasonic intensity was 0.5 W/cm^2, and the piezoelectric voltage reached ~0.35 V when the ultrasound intensity was further increased to 1.0 W/cm^2 (Figure 2F). Short-time Fourier transform analysis and spectral analysis confirmed that the frequency distribution of the measured piezoelectric output signal was concentrated at approximately 1 MHz, which was consistent with the applied ultrasonic frequency, confirming that PLLA could respond well to US (Figures 2G and 2H).

Design, fabrication, and characterization of ND-SENS

The fabrication of the biohybrid ND-SENS relied on the combination of PLLA membranes with ectodermal properties and living cells and included the following steps (Figure 3A): (1) MSCs

Please cite this article in press as: Shan et al., A neurodevelopment-inspired self-evolving scaffold for nerve regeneration, Cell Biomaterials (2024), https://doi.org/10.1016/j.celbio.2024.100006

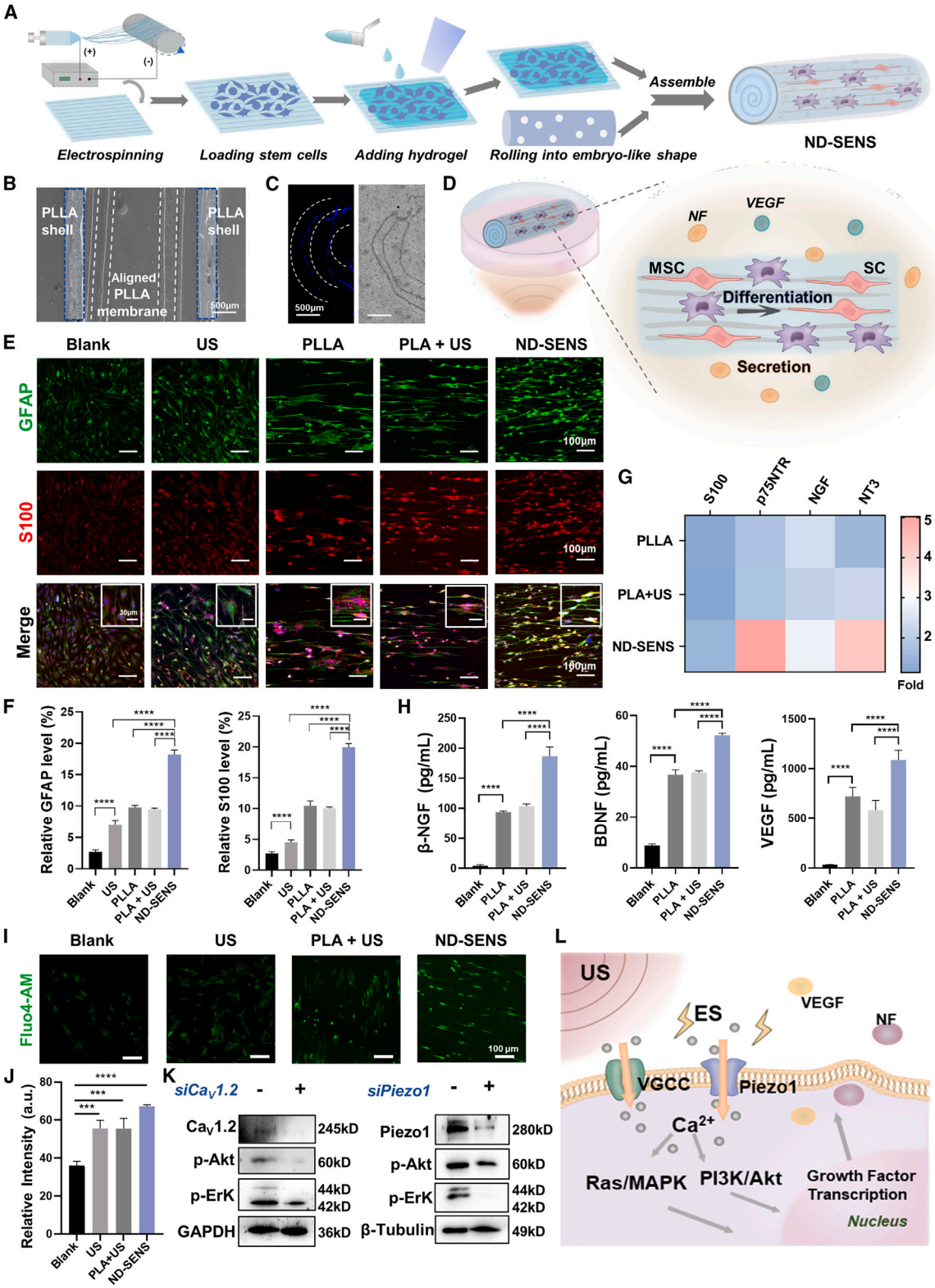

(legend on next page)

Please cite this article in press as: Shan et al., A neurodevelopment-inspired self-evolving scaffold for nerve regeneration, Cell Biomaterials (2024), https://doi.org/10.1016/j.celbio.2024.100006

were seeded on an unfolded PLLA fiber membrane; (2) light-cured hyaluronic acid methacrylate (HAMA) hydrogel was added to mimic the ECM; (3) the PLLA fiber membrane loaded with living cells was rolled into an embryo-like cylinder; (4) the prefabricated porous PLLA shell was assembled on the outside of the rolled hybrid membrane (Figure S6); and the stable biohybrid ND-SENS was finally obtained (the specific fabrication strategy is described in detail in the Methods section). Scanning electron microscopy (SEM) images of the cross-section along the long axis revealed that the ND-SENS exhibited an embryo-like multilayered structure consisting of a porous PLLA shell, a PLLA fiber membrane, and a living cell layer from the outside to the inside (Figure 3B). This embryonic-like encapsulation structure reduces the possibility of loaded stem cells migrating to the surrounding tissue or becoming inactivated in the implantation environment. The porous PLLA shell primarily served to provide support and protection. Following implantation, the shell could act as a nerve conduit, connecting the scaffold to the nerve stump and protecting the embryonic structure of ND-SENS from extrusion damage. In addition, the porous nature of the shell facilitated the exchange of substances and nutrients between the internal scaffold and the surrounding environment, thereby promoting the regeneration of neural tissue. To further confirm the cellular structure of the biohybrid system, the ND-SENS was cryosectioned perpendicular to its axis, and the nuclei were stained with Hoechst. The fluorescence image clearly revealed that the cells were arranged in a circle shape along the curling direction of the PLLA membrane (Figure 3C).

The biohybrid ND-SENS is composed of biosafe materials and living cells, so in principle, it should have excellent biocompatibility. CCK8 (cell counting kit 8) experiments and live/dead staining confirmed that PC12 cells (a rat medullary pheochromocytoma cell line) exhibited good activity when cocultured with separate single components of ND-SENS (the PLLA fiber membrane and HAMA hydrogel) or with the entire ND-SENS, with no significant difference compared with the activity of cells cultured in tissue cell plates (TCPs) (Figure S7). The long-term biosafety of the ND-SENS after implantation was then verified *in vivo*. When the ND-SENS was implanted into the sciatic nerve of rats for 3 months, the HE staining results of different tissues of rats (the heart, liver, spleen, lungs, and kidneys) showed no significant differences upon comparison with normal tissues from the blank group, demonstrating that the ND-SENS has excellent histocompatibility (Figure S8). In addition, the degradability of the materials contained within the ND-SENS was evaluated (Figure S9). The HAMA hydrogel took approximately 30 days to degrade *in vitro*, whereas for the porous shell and fiber membrane made of PLLA, weight reduction and degradation occurred at approximately the third to fourth months. The entire system was completely degraded within 12 months. As described above, the ND-SENS can generate a piezoelectric field under US to simulate the endogenous electric field of the ectoderm. To identify treatment parameters that are appropriate and safe, the effects of different US intensities on animals were evaluated. Figure S10 shows the simulated vibration of the composite plane of the PLLA membrane and hydrogel under different ultrasound intensities, as well as the results of a CCK8 assay with PC12 cells in different culture systems. For *in vitro* culture, the application of ultrasound at an intensity of 0.5 W/cm^2 did not affect cell viability; however, as the ultrasound intensity increased to 1.0 W/cm^2 or higher, cell viability decreased. Interestingly, the piezoelectric field generated by the ultrasound-excited ND-SENS was also found to promote the differentiation of neuronal cell lines (PC12 cells) into neurons (Figure S11). Compared with the TCP culture group (35.16 ± 8.75 μm), implantation of the PLLA membrane combined with the application of US at an intensity of 0.5 W/cm^2 significantly promoted the directional axon growth of PC12 cells (156.37 ± 35.54 μm).

The physical microenvironment created by the ND-SENS promoted the differentiation and secretion of loaded seed stem cells

During neural development, the endogenous electric field generated by the ectoderm stimulates neuroepithelial cells to differentiate into neural precursors, and ultimately differentiate into neurons and glial cells.[17,23] MSCs were used as "seed cells" in our biohybrid ND-SENS because MSCs have a wide range of sources, are easy to extract and isolate, and have low immunogenicity. Also, more importantly, they have the potential to differentiate into Schwann cells (SCs) as repair helper cells. Differentiated SCs could release neurotrophic factors and form Büngner bands at the injured site, thereby promoting axon regeneration in damaged nerve segments. Notably, SCs were not used directly in the ND-SENS. Instead, stem cells were selected because they

Figure 3. The embryonic endogenous electric field simulated by the ND-SENS promotes the differentiation and secretory activity of loaded stem cells

(A) Schematic diagram of the ND-SENS fabrication process.
(B) SEM image of longitudinal sections of the ND-SENS.
(C) Fluorescence microscopy image of loaded cells and SEM image of the cross-section of the ND-SENS.
(D) Schematic diagram showing the effect of the ND-SENS on loaded cells under US.
(E) Representative images of GFAP and S100 immunostaining in MSCs from the blank, US, PLLA, PLA + US and ND-SENS groups.
(F) Statistical analysis of relative GFAP and S100 levels in the five groups (n = 3).
(G) Relative gene expression levels of S100, p75NTR, NGF, and NT3 in the PLLA group, PLA + US group and ND-SENS group (n = 3).
(H) Concentrations of secreted neurotrophic factors β-NGF, BDNF, and VEGF in the different groups determined by ELISA (n = 3).
(I) Fluorescence labeling images of intracellular Ca^{2+} in the MSCs of different groups.
(G) Statistical analysis of the relative fluorescence intensity from labeled Ca^{2+} (n = 3).
(K) Western blotting of $Ca_v1.2$, Piezo1, p-Akt, and p-ErK expression levels in MSCs before and after the knockdown of $Ca_v1.2$ and Piezo1via siRNA.
(L) Schematic diagram of the molecular mechanism underlying the effects of the ND-SENS on loaded MSCs.
In (F)–(H), and (G), data are presented as mean ± SD. In (F)–(H), and (G), statistical significance was determined by the one-way ANOVA, $^*p < 0.05$, $^{**}p < 0.01$, $^{***}p < 0.001$, $^{****}p < 0.0001$.

Please cite this article in press as: Shan et al., A neurodevelopment-inspired self-evolving scaffold for nerve regeneration, Cell Biomaterials (2024), https://doi.org/10.1016/j.celbio.2024.100006

secrete cytokines relevant to differentiation, which is more conducive to inducing the recruitment and differentiation of endogenous stem cells. At the same time, the nutritional factors secreted by exogenous stem cells can serve as supplements to further promote repair. On the other hand, directly introducing SCs into a nerve repair scaffold also has many limitations, such as a low survival rate and a long culture cycle.

To verify whether the piezoelectric electric field generated by PLLA in the ND-SENS can promote the neural phase differentiation of stem cells *in vitro* similar to the endogenous electric field of the embryo (Figure 3D), the unfolded structure of ND-SENS was used to facilitate two-dimensional cell culture and observation, accompanied by US twice a day for 14 consecutive days to generate a piezoelectric field (ND-SENS). The Brunauer-Emmett-Teller (BET) porosity tests showed that the surface area of PLLA was 17.7680 m^2/g, and its BJH adsorption average pore diameter (4V/A) was 4.5091 nm (Figure S12). The nanopore structure provided by PLLA was conducive to cell adhesion and nutrient transfer. In comparison, MSCs cultured on TCP with US (the US group), cultured on PLLA membranes (the PLLA group), and cultured on nonpiezoelectric PLA membranes with US (the PLA + US group) were used as control groups (a detailed description of the grouping conditions is provided in the Methods section), whereas MSCs cultured directly in TCP served as the blank group. The results of immunofluorescence staining for glial fibrillary acidic protein (GFAP) and S100 (SC markers) after 14 days of coculture are shown in Figure 3E. Analysis of the cell morphology revealed that cells seeded on the fiber membrane exhibited a directional arrangement, which was attributed to the induction of cell growth by the ordered fiber structure on the membrane surface. In particular, the cells in the ND-SENS group exhibited spindle-shaped like growth with extended axons, which is similar to morphology of neural lineages such as glial cells and neurons. In terms of the expression levels of SC-specific proteins, the proportions of GFAP-positive cells and S100-positive cells followed the same trend under different culture conditions (Figure 3F). The blank group, which consisted of cells cultured in TCP alone, presented the lowest proportion of cells expressing GFAP and S100 ($GFAP^+$, 2.70% ± 0.32%; $S100^+$, 2.69% ± 0.32%); in comparison, the cells in the US group presented slightly higher proportions of cells expressing GFAP (7.04% ± 0.66%) and S100 (4.51% ± 0.39%), which might be because mechanical US promoted the directional differentiation of MSCs to a certain extent by activating mechanosensitive ion channels. In the PLLA group and PLA + US group, the ordered surface topological structures induced MSC differentiation into SCs through mechanical feedback from the matrix to the cells. Therefore, although neither group generated electrical signals, these groups had similar marker expression levels that were higher than those of the blank group. Under the action of the ultrasound-excited piezoelectric field, the proportions of $GFAP^+$ cells (18.20% ± 0.73%) and $S100^+$ cells (19.96% ± 0.59%) in the ND-SENS group increased by 86.51% and 90.96%, respectively, compared with those in the PLLA group, confirming that the simulated endogenous electrical environment was beneficial for the differentiation of stem cells into neural cells. Real-time qPCR was used to further quantify the differentiation of MSCs at the transcriptional level. The increased expression of S100 and p75NTR-related genes, which are markers of SCs, indicated the transdifferentiation of MSCs into SCs, whereas nerve growth factor (NGF) and neurotrophin-3 (NT3) are two neurotrophic factors secreted by glial cells (the sequences of these genes are shown in Table S2). The qPCR results were visualized via a heatmap (Figure 3G) showing relative fold differences in the expression levels of key mRNAs between the three groups of cells grown on the fibrous membranes (PLLA, PLA + US, and ND-SENS) and the blank group. Compared with those in the blank group, the expression levels of neurogenic differentiation-associated markers in MSCs in the three groups were all upregulated. Notably, among the three groups, the ND-SENS group presented the highest expression levels of the four related genes (vs. the blank group: S100, 1.45 ± 0.24-fold; p75NTR, 5.02 ± 2.84-fold; NGF, 2.79 ± 0.15-fold; and NT3, 4.26 ± 0.93-fold). The above results indicate that the ultrasonic field, the ordered surface topology of the substrate, and especially the simulated endogenous electric field based on the piezoelectric effect together constitute a microenvironment that promotes the neurogenic differentiation of stem cells.

Paracrine signals serve as key chemical signals for embryonic induction. Endogenous bioelectric fields are also known to affect the paracrine signaling of cells.[16,18] To determine whether the piezoelectric field generated by the PLLA in ND-SENS can regulate the paracrine effects of stem cells, enzyme-linked immunosorbent assay (ELISA) was used to evaluate the expression levels of relevant cytokines in the cell culture medium during differentiation (Figure 3H). Compared with those in the blank group, the expression levels of β-NGF, brain-derived neurotrophic factor (BDNF), and vascular endothelial growth factor (VEGF) in the PLA + US group, PLLA group, and ND-SENS group were significantly greater. Compared with the expression levels of these proteins in the PLLA group, which contained the same cell substrate without an electrical environment (β-NGF 93.55 ± 1.95 pg/mL; BDNF 36.68 ± 1.99 pg/mL; and VEGF 720.77 ± 89.85 pg/mL), the generated piezoelectric electric field significantly increased the secretion of these three nutritional factors in the ND-SENS group (β-NGF 186.53 ± 15.44 pg/mL; BDNF 52.20 ± 0.89 pg/mL; and VEGF 1,086.68 ± 96.92 pg/mL). In contrast, in the PLA + US group, with the presence of only ultrasound fields without electric fields had difficulty in promoting a significant increase in the secretion of trophic factors by MSCs (β-NGF 103.08 ± 4.03 pg/mL; BDNF 37.59 ± 0.63 pg/mL; and VEGF 581.96 ± 97.56 pg/mL). The above results verify the importance of simulating the endogenous electrical environment to promote paracrine effects.

The molecular mechanism underlying the increase in stem cell differentiation and secretion promoted by the ND-SENS was systematically studied. Ca^{2+} plays an important role as a promoter and mediator in various cellular processes in living cells, including the regulation of cell proliferation and death, enzyme and hormone synthesis, and the secretion of cytokines and neurotransmitters.[33,34] The piezoelectric field generated by the ND-SENS under US might have activated calcium ion-related ion channels and regulated the differentiation and secretory behavior of MSCs by changing the intracellular calcium ion concentration. Therefore, we first investigated the effect of the

Please cite this article in press as: Shan et al., A neurodevelopment-inspired self-evolving scaffold for nerve regeneration, Cell Biomaterials (2024), https://doi.org/10.1016/j.celbio.2024.100006

microenvironment constructed by the ND-SENS on the flow of calcium ions in stem cells. The fluorescence probe fluo-4 acetoxymethyl ester (Fluo 4-AM) was used to quantitatively analyze fluctuations in calcium ion levels in individual cells (Figure 3I; Video S1). Immediately after the application of US, the cells in the ND-SENS group presented the highest fluorescence signal, indicating a significant increase in the intracellular calcium ion concentration; in contrast, the intracellular fluorescence of the US group and the PLA + US group, which did not generate electrical signals, was slightly greater than that of the blank group, but far from the level of the ND-SENS group (Figure 3J). Curves showing the fluctuations in fluorescence intensity are shown in Figure S13. Electrical stimulation and mechanical vibration can act on the voltage-gated calcium channel (VGCC) protein $CaV_{1.2}$ and the mechanosensitive channel protein Piezo1, respectively to trigger calcium influx, thereby activating the downstream Ras/mitogen-activated protein kinase (MAPK) and phosphatidylinositol 3-kinase (PI3K)/protein kinase B (Akt) signaling pathways to promote the differentiation and secretory activity of MSCs.[35] Western blotting was then used to confirm that the physical microenvironment created by the ND-SENS regulated the expression of downstream proteins by acting on calcium-related membrane proteins in MSCs (Figure 3K). Compared with those in the PLLA group and the PLA + US group, the levels of phosphorylated Akt (p-Akt) and phospho-extracellular signal-regulated kinase (p-Erk) in the ND-SENS group were significantly greater (Figure S14). When the ND-SENS group was cocultured with small interfering RNA (siRNA) (siPiezo or si$CaV_{1.2}$) to knock down the expression of the mechanosensitive protein channel Piezo1 and the VGCC protein $CaV_{1.2}$, respectively, the levels of p-Akt and p-Erk in both groups decreased significantly (Figure 3K). The above data demonstrate that the ND-SENS simultaneously activated the membrane proteins Piezo1 and $CaV_{1.2}$ through simulated endogenous electric fields and accompanying US, thereby increasing the intracellular Ca^{2+} concentration and activating the downstream Ras/MAPK and PI3K/Akt signaling pathways, ultimately promoting the differentiation of MSCs into SCs and the secretion of neurotrophic factors (β-NGF and BDNF) as well as VEGF (Figure 3L).

ND-SENS can recruit surrounding stem cells and affects the growth of neural tissue *in vitro*

The biomimetic endogenous electric field generated by ND-SENS promoted not only the directional differentiation of internally loaded exogenous MSCs at the injury site but also the secretion of repair-promoting cytokines; more importantly, the paracrine effect enhanced by the electric field promoted the recruitment of endogenous stem cells, providing the material basis for the rapid repair of neural tissue. The ability of ND-SENS to recruit stem cells was evaluated via a Transwell assay (Figure 4A). As shown in Figure 4B, the cylindrical three-dimensional ND-SENS was placed in the lower chamber of the Transwell to simulate its implantation at the injury site, and an electric environment simulating the ectoderm was generated by applying US. Simultaneously, MSCs were seeded on the upper layer of the Transwell to simulate the surrounding endogenous stem cells. Crystal violet staining revealed that, compared with the blank group, the experimental group in which the ND-SENS placed in the lower chamber recruited more cells from the upper chamber (197.66 ± 43.10); in particular, compared with that in the control group without (w/o) US (i.e., ND-SENS w/o US) (296.33 ± 27.06), the number of migrating cells in the ND-SENS group was significantly greater (485.33 ± 8.14) (Figure 4C). These results demonstrated that the embryonic-like microenvironment simulated by the ND-SENS has the potential to promote endogenous stem cell recruitment.

The ND-SENS was demonstrated to successfully regulate the morphology and function of loaded exogenous stem cells the potential to recruit endogenous stem cells, thereby providing an excellent regenerative environment. DRGs are nodular structures where sensory neuronal cells accumulate outside the spinal canal. DRG are responsible for transmitting sensory information from the peripheral nervous system to the central nervous system. To further verify that the ND-SENS can promote nerve growth at the tissue level, DRG explants were placed in the ND-SENS and cocultured with MSCs *in vitro* for 10 days, after which immunofluorescence staining was used to observe nerve growth. In the TCP culture group, neuronal cells and glial cells grew in a network shape. In contrast, in the ND-SENS w/o US group, the axons extending from the DRG explant showed directional growth to a certain extent, with an average length of 2.91 ± 0.43 mm and a maximum length of 3.40 ± 0.11 mm, which was attributed to the induction of axon growth by the ordered micro/nanostructure on the surface of the PLLA membrane and the cylindrical spatial confinement structure formed by curling of the PLLA membrane (Figures 4D and 4E). Notably, radially growing cells were also observed in the background of the ND-SENS w/o US group. In addition, although some cells in the newly grown tissue presented neuron-specific class III beta-tubulin (Tuj1) expression, more cells expressed GFAP, a specialized marker of glial cells. In the ND-SENS group, the DRG explants grew highly oriented axons with the longest average length (3.90 ± 0.35 mm) and maximum length (4.30 ± 0.23 mm) and the highest proportion of Tuj1-positive cells, effects that were largely attributed to the recruitment and differentiation induction of MSCs in the culture environment induced by ND-SENS (Figure 4F). The above experiments confirmed that the ND-SENS promoted nerve growth at the tissue level, which was attributed to the embryo-like microenvironment constructed by the special morphology, ordered surface topology, and piezoelectric field formed under ultrasonic excitation of the ND-SENS.

The ND-SENS achieved nerve regeneration in rats with a sciatic nerve defect

As a functional implant, ND-SENS must meet the following two prerequisites: (1) its mechanical properties should be similar to those of nerves and (2) it should remain stable under physiological conditions for a period of time without being degraded too quickly. The stress-strain curve obtained by static tensile experiment confirmed that the unfolded ND-SENS film possessed excellent toughness similar to that of nerves (Figure S15). Dynamic mechanical analysis (DMA) results showed that the energy storage modulus of unfolded ND-SENS film was relatively stable during dynamic stretching, indicating good deformation and resilience (Figure S16). Further, stability tests of ND-SENS in phosphate buffered saline (PBS), simulated body fluids (SBFs), and complete medium showed that their quality and morphology

Please cite this article in press as: Shan et al., A neurodevelopment-inspired self-evolving scaffold for nerve regeneration, Cell Biomaterials (2024), https://doi.org/10.1016/j.celbio.2024.100006

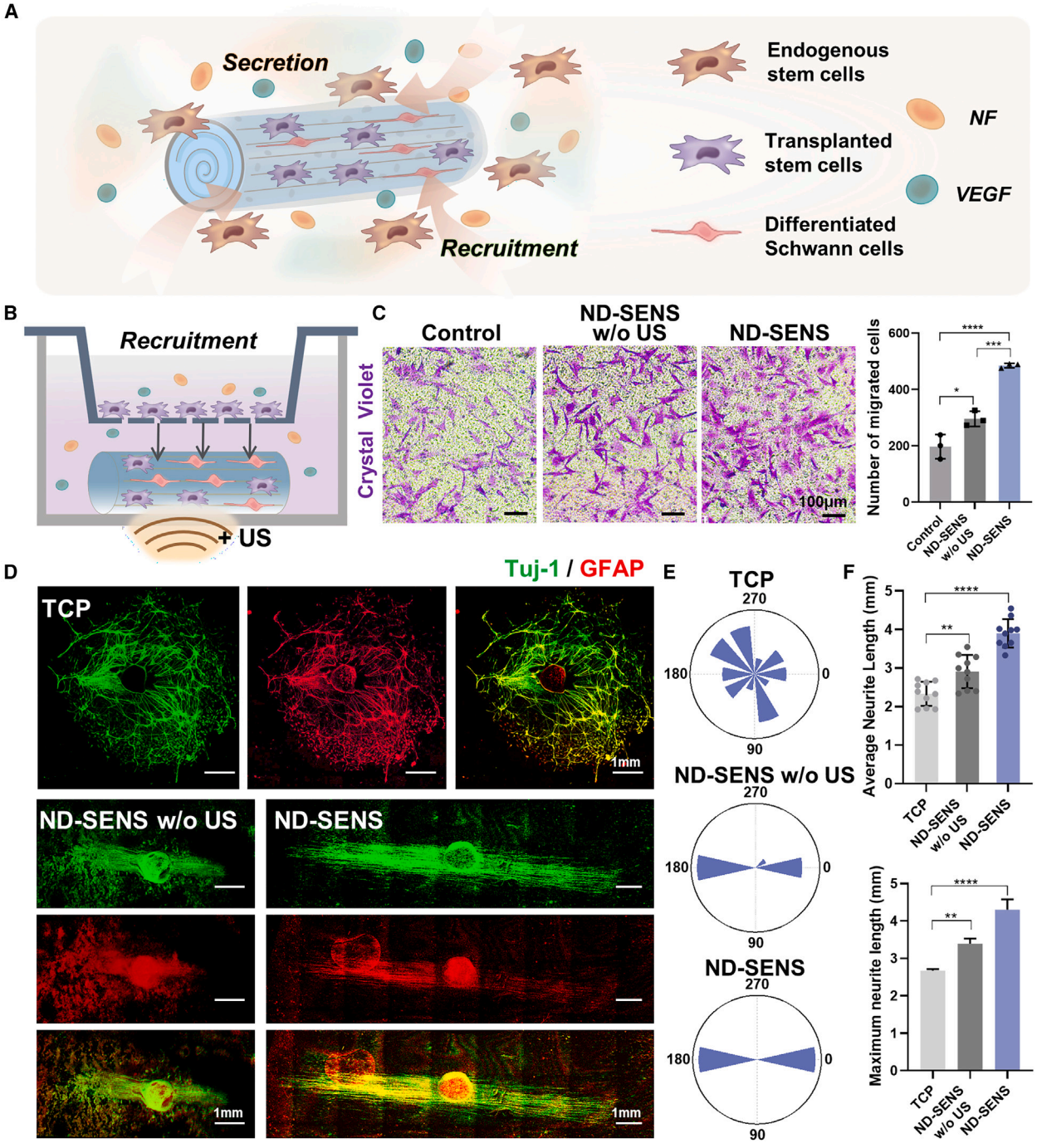

Figure 4. The ND-SENS can recruit stem cells and promote the growth of tissue explants

(A) Schematic diagram showing the ability of the ND-SENS to recruit endogenous stem cells through paracrine signals.
(B) Schematic diagram showing a Transwell experiment designed to evaluate endogenous stem cell recruitment.
(C) Crystal violet staining of MSCs and statistical analysis of the number of cells in each field of view (n = 3).
(D) Images of the growth status of DRG explants in the different experimental groups, where green represents the neuronal indicators Tuj1 and red represents the SC indicator GFAP.
(E) Statistical analysis of the growth of DRG axons.
(F) Statistical analysis of the average length and maximum length of DRG axons (n = 3).
In (C) and (F), data are presented as mean ± SD. In (C) and (F), statistical significance was determined by the one-way ANOVA, (B), (D), (F), and (H),*$p < 0.05$, **$p < 0.01$, ***$p < 0.001$, ****$p < 0.0001$.

Please cite this article in press as: Shan et al., A neurodevelopment-inspired self-evolving scaffold for nerve regeneration, Cell Biomaterials (2024), https://doi.org/10.1016/j.celbio.2024.100006

CellPress
OPEN ACCESS

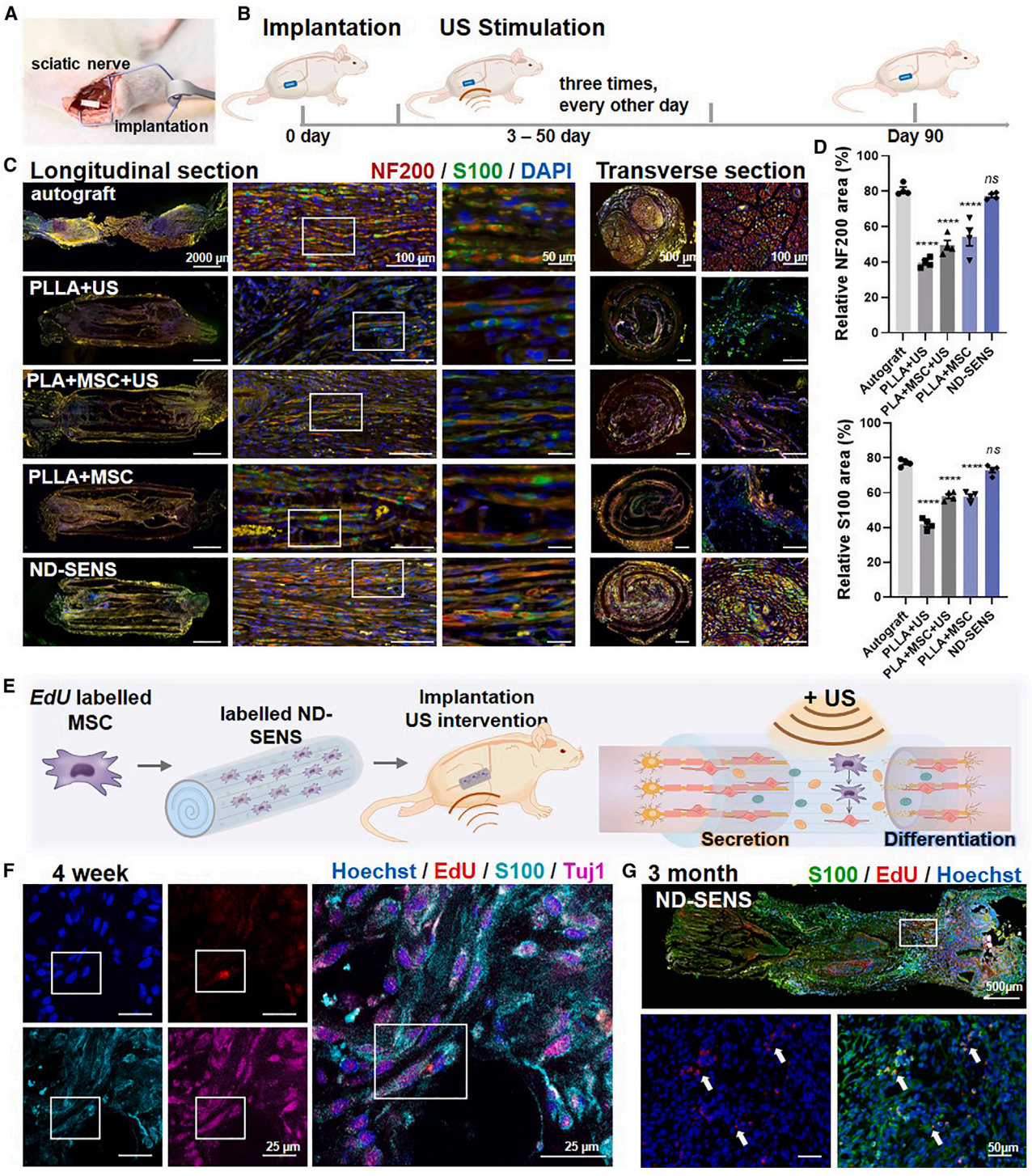

Figure 5. The ND-SENS successfully achieved *in situ* nerve repair in rats with PNI

(A) Surgical images of the ND-SENS implanted in a rat with PNI.

(B) Schematic diagram of the ND-SENS treatment process.

(C) Representative immunofluorescence staining images of transverse/longitudinal tissue sections of the regenerated sciatic nerve; the red fluorescent signal represents NF200 and the green fluorescent signal represents S100.

(D) Statistical analysis of the relative fluorescence from NF200 and S100 (n = 4).

(E) Schematic diagram of an experiment used to track loaded exogenous stem cells.

(legend continued on next page)

Please cite this article in press as: Shan et al., A neurodevelopment-inspired self-evolving scaffold for nerve regeneration, Cell Biomaterials (2024), https://doi.org/10.1016/j.celbio.2024.100006

remained stable over a period of 15 days (Figure S17). The above results confirmed that ND-SENS could stably adapt to defective nerve tissue. To verify the ability of the ND-SENS to reconstruct an embryonic-like physical and chemical microenvironments to achieve nerve regeneration *in vivo*, a rat sciatic nerve defect model was established. SD rats underwent surgery to remove 1 cm of the sciatic nerve, and then nerve autografts and nerve scaffolds prepared under different conditions were then transplanted into the defect area respectively (Figure 5A). All the model rats were randomly divided into five treatment groups: nerve autograft group, PLLA + US group, PLLA + MSC scaffold group, PLA + MSC + US scaffold group, and ND-SENS group. The rats in the PLA + MSC + US and ND-SENS groups received ultrasound stimulation 3 days after scaffold implantation, and then received US three times every other day until 50 days after implantation (Figure 5B). 3 months after implantation, nerve tissue samples were dissected, and the tissue sections were fluorescently stained for the mature neuron marker-neurofilament-200 (NF200), the SC marker-S100, and the nuclear marker DAPI. As shown in Figure 5C, there was a certain amount of NF200 and S100 expression was observed in the regenerated nerves at the primary injury site in each experimental group, indicating that varying degrees of nerve repair occurred in each treatment group. Furthermore, there was no significant difference in the expression levels of the NF200 or S100 proteins in the autograft group (NF200: 80.75% ± 2.76%, S100: 77.22% ± 1.77%) or the ND-SENS group (NF200: 77.39% ± 1.71%, S100: 72.98% ± 2.54%), and both groups showed significantly increased marker expression compared with that in the other experimental groups (NF200: PLLA + US, 39.77% ± 2.36%; PLA + MSC + US, 49.60% ± 4.64%; PLLA + MSC, 54.26% ± 8.70% S100: PLLA + US, 42.02% ± 2.76%; PLA + MSC + US, 58.02% ± 2.25%; PLLA + MSC, 57.79% ± 2.44%) (Figure 5D). Moreover, we also found that the co-localization level of the two proteins was higher in the ND-SENS group, and the periphery of the $NF200^+$ region was enclosed by $S100^+$ regions, indicating that the embryonic-like microenvironment provided by the ND-SENS promoted the self-development of nerves and ultimately achieved axonal regeneration and remyelination. In addition, when the tissue anatomy was examined, the ND-SENS group showed excellent nerve repair effects, reaching a level comparable to that of the group administered autograft transplantation, the gold standard treatment. Other treatment groups (the PLLA + US group, PLA + MSC + US group, and PLLA + MSC group) were unable to simulate endogenous electrical signals similar to those of the ND-SENS group; therefore, nerve regeneration in these groups after treatment was insufficient, and the degree of axonal remyelination was relatively low.

In addition to providing the physical signals of embryonic induction, the ND-SENS can induce the recruitment of endogenous stem cells by enhancing secretion to simulate paracrine chemical signaling, thereby achieving the synergistic repair of defective tissues. To further study the cellular dynamic process by which the ND-SENS promotes neural tissue regeneration, labeling with the nucleoside analog ethoxyuridine (EdU) was used to monitor the distribution and fate of loaded MSCs after ND-SENS implantation *in vivo* (Figure 5E). Immunofluorescence staining and flow cytometry confirmed that 98% of the MSCs were successfully labeled with the fluorescent probe EdU (Figure S18). Then the EdU-labeled MSCs were used to prepare a biohybrid ND-SENS that was implanted into rats with sciatic nerve defects. 4 weeks after implantation, immunofluorescence staining images of regenerated nerve tissue sections revealed that the EdU^+ cells also colocalized with $S100^+$ cells, indicating that the MSCs in the ND-SENS group had already differentiated into SCs in the rats (Figure 5F). 3 months after implantation, immunofluorescence staining of the regenerated nerve tissue revealed that the EdU^+ cells were arranged along the direction of nerve extension and colocalized with $S100^+$ cells (Figure 5G). However, interestingly, the majority of $S100^+$ cells, representative of SCs, were EdU negative, indicating that the regenerated neural tissues were mostly derived from the recruitment and differentiation of endogenous stem cells.

The ND-SENS effectively repaired peripheral nerve damage by restoring the nanostructure, the tissue structure, and motor function

To further illustrate the myelination level of the regenerated nerves, transmission electron microscopy (TEM) was used to observe the micro/nanostructure of the regenerated nerve tissue. TEM images showed that compared with the other experimental groups (Figure 6A), the ND-SENS group presented the largest axon diameter (5.52 ± 0.88 μm) and the thickest regenerative myelin sheath wrapping (0.70 ± 0.19 μm), indicating myelin regeneration close to that in the autograft group (axon diameter: 5.61 ± 1.48 μm and myelin thickness: 0.71 ± 0.07 μm) (Figure 6B).

Sciatic nerve injury can seriously affect the physiological state of the innervated muscles, thereby affecting the motor function of the hind limbs. Therefore, we further evaluated whether the ND-SENS could improve muscle status and restore the motor ability of rats through neural repair. Histological analysis of the gastrocnemius muscle revealed that the right leg muscle with nerve damage in the untreated blank group presented varying degrees of morphological atrophy, accompanied by significant changes in muscle weight (Figures 6C and 6D). After 3 months of treatment with autografts and the ND-SENS, the shape and weight had nearly returned to normal levels (muscle weight difference: 0.95 ± 0.07 g for the ND-SENS group and 0.65 ± 0.05 g for the autograft group). Masson staining of the gastrocnemius muscle tissue revealed that the collagen fiber contents in the muscles of the autologous transplantation group and the ND-SENS group was lower than that in the PLLA + US, PLA + MSC + US, and PLLA + MSC groups, indicating that the ND-SENS effectively improved muscle atrophy and reduced

(F) Representative fluorescence staining results of regenerative nerve tissue sections 4 weeks after implantation of the ND-SENS prepared with EdU-labeled exogenous stem cells; blue represents Hoechst, red represents EdU, cyan represents S100, and magenta represents Tuj1.
(G) Representative fluorescence staining results of regenerated nerve tissue sections 3 months after implantation of the ND-SENS prepared with EdU-labeled exogenous stem cells.
In (D), data are presented as mean ± SD. In (D), statistical significance was determined by the one-way ANOVA, ****$p < 0.0001$.

Please cite this article in press as: Shan et al., A neurodevelopment-inspired self-evolving scaffold for nerve regeneration, Cell Biomaterials (2024), https://doi.org/10.1016/j.celbio.2024.100006

CellPress
OPEN ACCESS

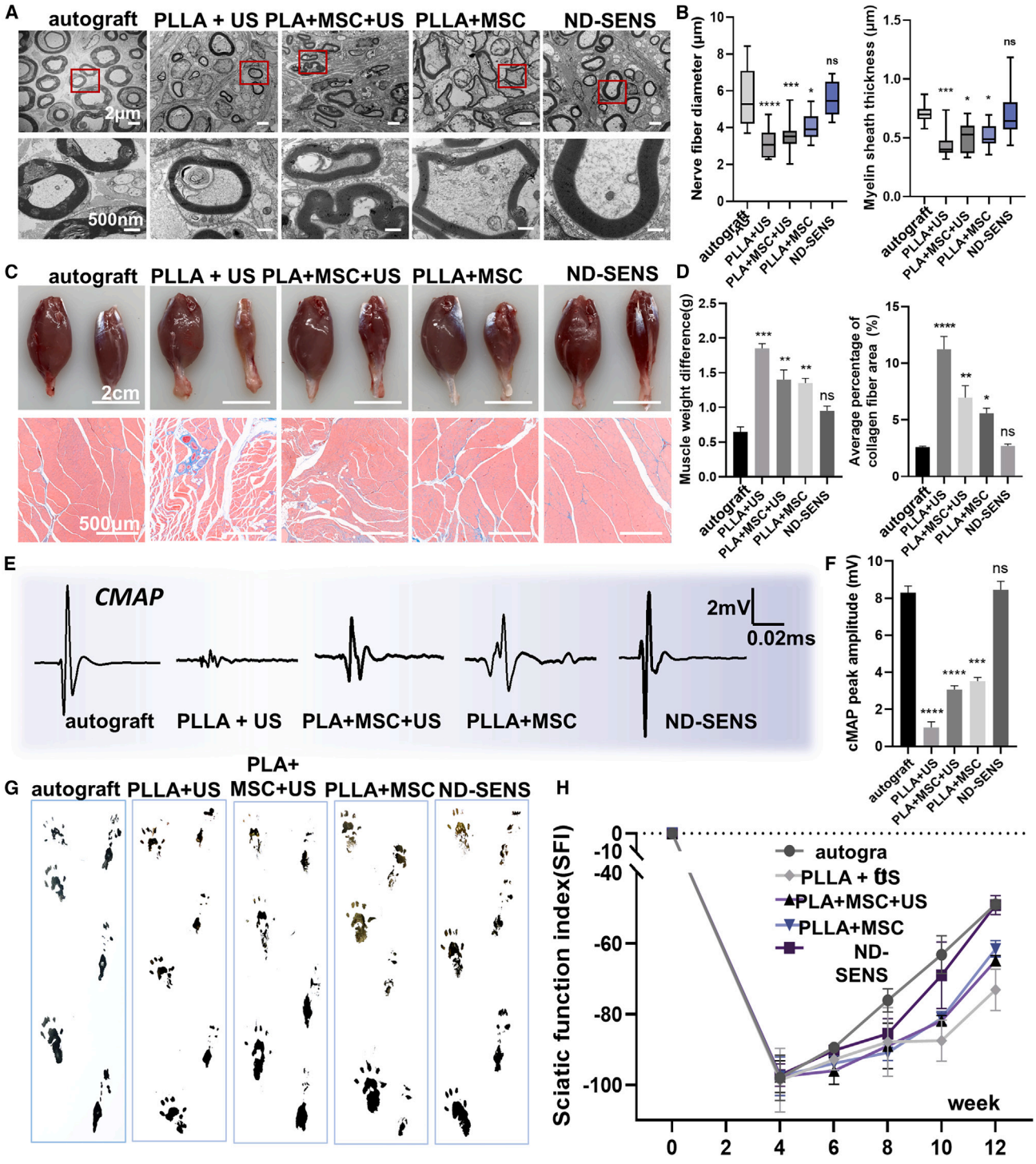

Figure 6. The ND-SENS restored nerve conduction and motor function in rats with PNI

(A) Representative TEM images of the myelinated axonal regrowth in the five experimental groups.

(B) Quantitative analysis of the nerve fiber diameter and myelin sheath thickness (n = 10).

(C) Representative images of the gastrocnemius muscles of rats in different treatment groups and Masson staining results of the right gastrocnemius muscles in each group.

(D) Statistical analysis of the difference in muscle weight between the left and right legs and the average collagen fiber area percentage of each experimental group (n = 3).

(legend continued on next page)

Please cite this article in press as: Shan et al., A neurodevelopment-inspired self-evolving scaffold for nerve regeneration, Cell Biomaterials (2024), https://doi.org/10.1016/j.celbio.2024.100006

muscle tissue inflammation (Figures 6C and 6D). To further evaluate the function of the innervated muscles, the composite muscle action potential (CMAP) tests were performed with the injured hind limb (Figure 6E). The ND-SENS group (8.46 ± 0.32 mV) presented a high level of CMAP similar to that of the autograft group (8.31 ± 0.26 mV) (Figure 6F). Finally, the recovery of motor function after nerve repair was evaluated through gait analysis (Figure 6G). During the 3-month repair process, the sciatic nerve function index (SFI) of the ND-SENS group (−49.11 ± 2.17) was closer to that of the autologous transplantation group (−48.89 ± 0.99), and the rate of motor function recovery after sciatic nerve injury in rats was faster in the ND-SENS group than in the other groups (Figure 6H).

Transcriptome analysis to assess the molecular mechanism by which the ND-SENS repairs PNI

To explore the molecular mechanism by which the ND-SENS promotes neural repair by simulating embryonic-induced physical and chemical signals in greater detail, we sequenced the transcriptomes of repaired neural tissues from five different experimental groups. Differential gene expression among the groups was evaluated, and the results are shown in Figure S19. When all the experimental groups were compared, the difference in gene expression was smallest for the ND-SENS group and the autograft group, indicating that the ND-SENS achieved therapeutic effects similar to those of the autograft. Heatmaps of the differentially expressed genes (DEGs) in the blank, autograft, PLLA + US, PLLA + MSC group, PLA + MSC + US, and ND-SENS group were further analyzed. Among all the differences in gene expression, the ND-SENS group presented the greatest difference in gene expression compared with the blank group and the smallest difference compared with the autograft group (Figure 7A).

The sets of DEGs between the ND-SENS group and the blank group were analyzed in detail. A volcano plot of differential gene expression (Figure 7B) revealed that 852 genes were upregulated, and 793 genes were downregulated between the ND-SENS group and the blank group. Among the upregulated genes, the Piezo1gene is related to mechanosensitive channels, the Cacna1b and Cacng4 genes are related to calcium ion channels, and the Rasd1, Rasl11a, Rasal3, Mapk13, Rhoh, and Mknk2 genes are related to the Ras-MAPK and PI3k Akt signaling pathways. Upregulation of the genes S100a8 and S100a9, which are related to myelin formation, was also observed. In addition, we performed kyoto encyclopedia of genes and genomes (KEGG) enrichment analysis and gene ontology (GO) enrichment analysis between the ND-SENS group and the blank group, and the results are shown in Figures 7C and 7D. The KEGG enrichment analysis revealed that the top ten terms enriched in the genes with significantly upregulated expression were ECM receptor interactions, axon guidance, cell adhesion factors, the PI3K-Akt signaling pathway, the Ras signaling pathway, the VEGF signaling pathway, the MAPK signaling pathway, the calcium ion signaling pathway, and neuroactive ligand-receptor interactions (Figure 7C). GO enrichment revealed that the top ten enriched terms were neuron projection guidance, myelination, cell morphogenesis, glial cell regeneration regulation, positive regulation of cell development, positive regulation of nervous system development, positive regulation of nerve regeneration, axonal guidance, and axonal myelin wrapping ranked in the top ten (Figure 7D). The above results confirmed that mechanism by which the ND-SENS regulates the majority of endogenous stem cells is consistent with the experimental results previously obtained with MSCs: the ND-SENS can activate calcium ion channels and mechanosensitive ion channels and achieve myelin regeneration by increasing the expression levels of genes related to Ras-MAPK and PI3k-Akt signaling pathways. The DEGs between the ND-SENS group and the blank group were used to prepare a protein-protein interaction network (Figure 7E), and we marked the proteins related to neural repair in red. In the network, the proteins marked in red are mostly in middle positions among the network and are highly likely to be nodes, and the probability of edges between these proteins and neighboring nodes is high, indicating the paracrine signals provided by the ND-SENS also play an important role in neural repair.

KEGG analysis of DEGs among other experimental groups was then carried out. As shown in Figure 7F, when DEGs between the piezoelectric scaffold group without MSCs (PLLA + US) and the biohybrid ND-SENS group were analyzed, the significantly enriched terms involved interactions between important proteins, cytokines, and cytokine receptors, demonstrating the importance of live seed cells in the ND-SENS. The introduced MSCs played a similar role to that of neuroepithelial cells during embryonic development to a certain extent, promoting the paracrine secretion of cytokines and recruiting endogenous stem cells under the action of the simulated endogenous embryonic electric field provided by the ND-SENS. Compared with the experimental groups that were loaded with exogenous stem cells without simulated endogenous electric fields (PLLA + MSC, PLA + MSC + US), the ND-SENS group showed significant enrichment in calcium ion signaling pathway activation, indicating that piezoelectric electric fields increased the activation level of calcium ion signaling pathways. GO analysis of the DEGs between the ND-SENS group and the other four groups also verified this conclusion (Figure S20).

To further validate the transcriptome sequencing data and confirm that the expression of downstream pathway-related genes was truly activated in the regenerated neural tissue in the ND-SENS group, we performed immunohistochemical analysis of the phosphorylated MAPK and Akt proteins (p-MAPK and p-Akt) in the regenerated neural tissue of each experimental group (the PLLA + US, PLLA + MSC, PLA + MSC + US, and

(E) Representative CMAP of different experimental groups after 12 weeks.
(F) Statistical analysis of the average CMAP amplitude of the different experimental groups (n = 3).
(G) Representative footprints of rats in the different experimental groups after treatment.
(H) SFI curves of the different experimental groups at 4, 6, 8, 10, and 12 weeks (n = 3).
In (B), (D), (F), and (H), data are presented as mean ± SD. In (B), (D), (F), and (H), statistical significance was determined by the one-way ANOVA, $^{*}p < 0.05$, $^{**}p < 0.01$, $^{***}p < 0.001$, $^{****}p < 0.0001$.

Please cite this article in press as: Shan et al., A neurodevelopment-inspired self-evolving scaffold for nerve regeneration, Cell Biomaterials (2024), https://doi.org/10.1016/j.celbio.2024.100006

CellPress
OPEN ACCESS

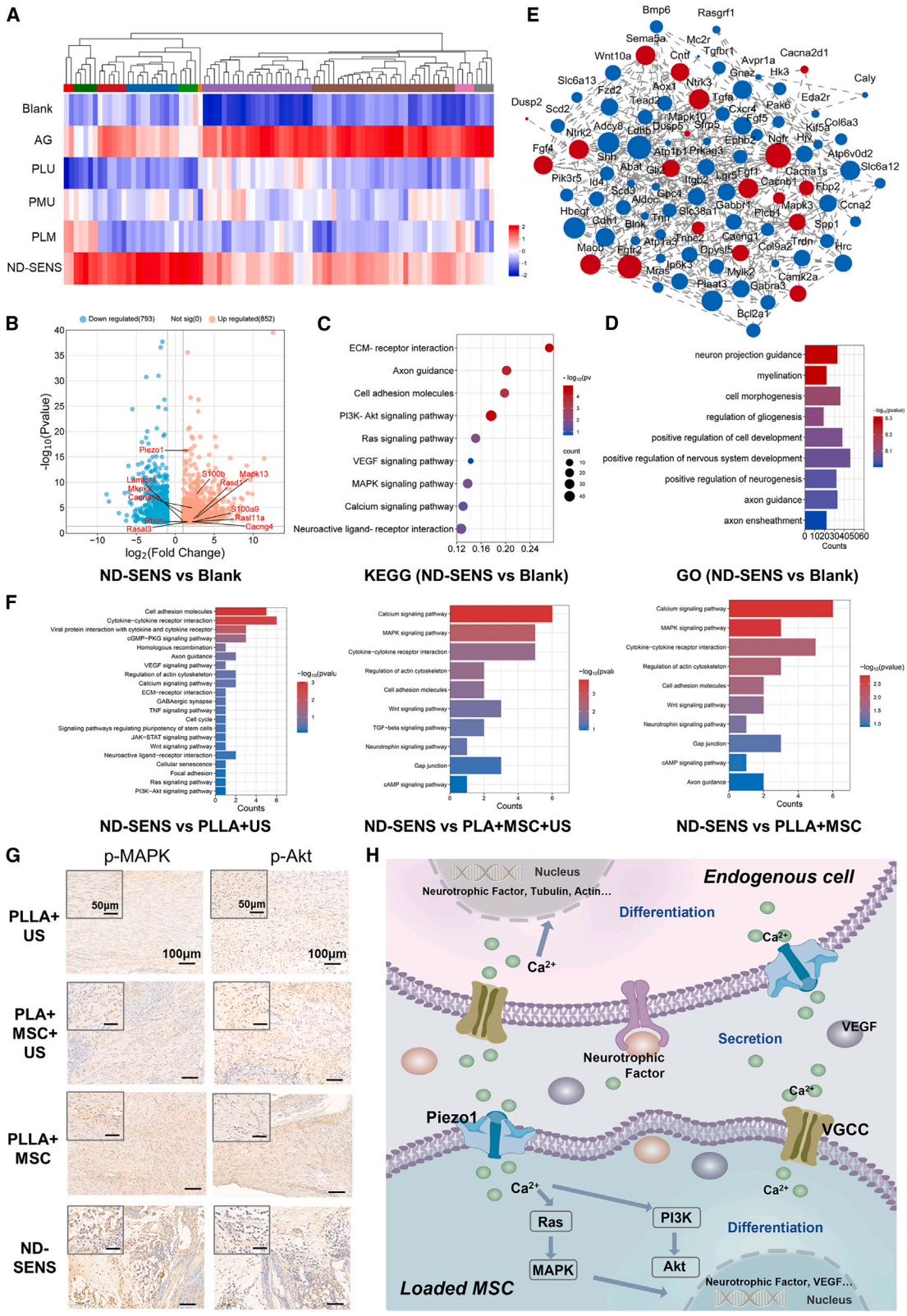

(legend on next page)

Please cite this article in press as: Shan et al., A neurodevelopment-inspired self-evolving scaffold for nerve regeneration, Cell Biomaterials (2024), https://doi.org/10.1016/j.celbio.2024.100006

ND-SENS groups). As shown in Figures 7G and S21, the levels of the p-MAPK and p-Akt proteins in the sciatic nerve tissue of rats in the ND-SENS group were significantly increased, consistent with the experimental results at the cellular level. Overall, the ND-SENS created ND-like environment involving simulated endogenous electric fields generated under US, as well as interactions between loaded exogenous stem cells and endogenous cells (Figure 7H). Piezoelectric fields and accompanying ultrasonic vibrations can activate the VGCC and Piezo1, respectively, leading to calcium ion influx in stem cells and subsequent activation of the downstream Ras-MAPK and PI3K-Akt signaling pathways, thereby increasing the expression of transcription factors related to differentiation and secretion.

Conclusions

PNI represents a significant global health concern that can restrict patients' daily activities, severely impair their quality of life, and place a significant burden on the healthcare system and society. Currently, implantation surgery based on scaffold materials is a potential effective strategy for repairing defective neural tissue. However, traditional neural scaffolds mainly guide the regeneration of defective neural tissue by constructing nerve fiber-like morphology and mechanical properties. Although this approach can promote cell migration and growth in a specific direction, it cannot effectively regulate the homing and differentiation of endogenous stem cells due to the lack of biological activity. Composite neural scaffolds incorporating cytokines can improve their bioactivity in the short term; however, they also have challenges s such as limited cytokine load, uncontrolled release, and easy degradation and inactivation. It is worth noting that in the design of scaffold materials, the simulation of multi-dimensional physical and chemical signals of the neural microenvironment is often easily overlooked, and these signals play a key role in the regeneration process. In particular, endogenous bioelectric signals are extremely important both for the development of the nervous system and for maintaining its physiological functions. Some prospective studies have also confirmed at the cellular level that electrical stimulation based on the deformation of the piezoelectric substrate can open the ion channels of cells, thereby activating signal pathways related to cell proliferation and migration. However, how to integrate piezoelectric materials into neural scaffolds and reconstruct a neural growth and development microenvironment with multi-dimensional signals remains a major challenge. In the present work, a SENS inspired by embryonic development is proposed; the biohybrid ND-SENS can mimic both the endogenous electrical environment and paracrine chemical signaling of the embryo. The ND-SENS constructs an embryo-like developmental environment that induces the recruitment of endogenous stem cells and acts on a VGCC protein and mechanosensitive channel protein, thereby activating the downstream Ras/MAPK and PI3K/Akt signaling pathways, and ultimately inducing the neural differentiation of recruited endogenous stem cells. Experiments in a rat sciatic nerve injury model confirmed that the ND-NENS exhibits excellent neurorestorative effects both histologically and functionally, similar to the effects of autologous nerve grafting. This development-inspired tissue engineering scaffold strategy opens up new possibilities in regenerative medicine.

Continued study of ND-SENS may provide some promising avenues for exploration and improvement in the field of tissue repair. First, although the ND-SENS has demonstrated promising outcomes in models of PNI, its efficacy in other complex clinical scenarios (e.g., large nerve gaps or central nerve injury) remains to be further investigated. Second, the therapeutic efficacy demonstrated based on embryonic developmental inspired ND-SEN makes it a promising candidate for application in other areas of tissue repair, including the musculoskeletal, skin, cardiac tissue, immunological, and vascular tissue.[36] Although the strategy used to prepare the ND-SENS proposed described in this article may not be optimal for the regeneration of other tissues, and it may be necessary to replace seed cells or select scaffold materials with different electrical output properties and micro/nanostructures. A further area meriting detailed investigation is the long-term durability and stability of ND-SENS implants. A comprehensive understanding of the degradation kinetics of scaffolds and their ability to maintain structural integrity over extended periods is essential for accurately predicting and optimizing their therapeutic lifespan, which is necessary for further clinical applications and expansion into other tissue repair areas. Additionally, the fabrication of ND-SENS involves the preparation of PLLA and gels, as well as MSCs seeding. Consequently, robust manufacturing processes and rigorous quality control measures must be implemented to facilitate the transition from preclinical studies to widespread clinical use and to ensure the safety and efficacy of the product across diverse patient populations.

METHODS

Materials

PLLA powder and PLA powder (molecular weight: 260,000) were purchased from Daigang biomaterial (China). Dichloromethane,

Figure 7. Molecular mechanism by which the ND-SENS repairs the injured sciatic nerve in rats determined on the basis of transcriptomic analysis

(A) Heatmaps showing differential gene expression between the blank group and other experimental groups.
(B) Volcano maps of differential expression genes in the ND-SENS group relative to the blank group.
(C) Bubble plots of KEGG pathways enriched in the differentially expressed genes in the ND-SENS group relative to the blank group.
(D) Bar plots of GO terms enriched in the differentially expressed genes in the ND-SENS group relative to the blank group.
(E) String interaction network of differentially expressed genes between the ND-SENS and blank group. The red dots represent the genes related to nerve repair.
(F) Bar plots showing KEGG pathways enriched in the differentially expressed genes in the ND-SENS group relative to the other experimental groups.
(G) Immunohistochemical images of p-MAPK and p-Akt in the regenerated sciatic nerve tissue of rats in the PLLA + US, PLA + MSC + US, PLLA + MSC, and ND-SENS groups.
(H) Schematic diagram of the molecular mechanism by which the of ND-SENS repairs sciatic nerve injury in rats.

Please cite this article in press as: Shan et al., A neurodevelopment-inspired self-evolving scaffold for nerve regeneration, Cell Biomaterials (2024), https://doi.org/10.1016/j.celbio.2024.100006

trichloromethane, and hexafluoroisopropanol solvent were obtained from Aladdin (China). The alpha minimal essential medium (α-MEM) and fetal bovine serum (FBS) were purchased from Gbico (USA). 4% Paraformaldehyde (PFA), 1% penicillin-streptomycin, Triton X-100, DAPI, rat tail tendon collagen type I, cell lysis buffer, Dulbecco's PBS (D-PBS), bicinchoninic acid kit (BCA kit) for protein quantification, PVDF membrane (0.22 μm), 10 × TBST solution, extremely sensitive chemiluminescent (ECL) reagent, GAPDH (glyceraldehyde-3-phosphate dehydrogenase) monoclonal antibody (K200057M), β-tubulin monoclonal antibody (K200059M), and goat serum were obtained from Solarbio (China). Anti-GFAP antibody (ab4684), anti-S100 beta antibody (ab52642), anti-beta III tubulin antibody (ab52623), anti-NF200 antibody (ab7794), goat anti-rabbit immunoglobulin G (IgG) H&L (Alexa Fluor 488, ab150077), and goat anti-mouse IgG H&L (Alexa Fluor 647, ab150115) were purchased from Abcam (UK). FastPure Cell/Tissue Total RNA Isolation Kit, HiScript II Q Select RT SuperMix for qPCR, and Taq Pro Universal SYBR qPCR Master Mix were obtained from Vazyme (China). Fluo 4-AM solution was purchased from Donjindo (Japan). Piezo1 antibody (15939-1-AP) was obtained from Proteintech (China). $Ca_V1.2$ (ACC-003) antibody was purchased from Alomone (Israel). Phospho-p44/42 MAPK (Erk1/2) antibody (4370) and phospho-Akt (4060) antibody from Cell Signaling Technology (USA). EdU detection kit, siRNA-Piezo1, and siRNA-$CaV_{1.2}$ were purchased from RiboBio (China). HAMA was purchased from Engineering for Life (China, EFL-HAMA-400K). 5-0 and 9-0 sutures were obtained from Jinhuan Medical Appliance (China).

Fabrication and characterization of PLLA-aligned piezoelectric film

0.5 g of PLLA (or PLA) powder and 6.2 g of hexafluoroisopropanol were put into a sample bottle and mixed on a magnetic stirring platform for 3 h to a solution with a mass fraction ratio of 7.5% (w/w). Then the solution was poured into a syringe with a number 20 needle and a voltage of 12 kV was added to the needle and a negative voltage of −3 kV was added to the receiver with an aluminum foil. The distance between the tip of the needle and the nanofiber receiver was 20 cm. At a receiver rotation speed of 800 r/min and an inlet speed of 1 mL/h, the PLLA film was produced by spinning for 30 min. The electrospinning box was enclosed and in an ultraviolet irradiated space. After electrospinning, the PLLA film was removed from the receiver, placed in a sterile dish, transferred to a vacuum drying oven, and dried in a vacuum oven at 40°C for 8 h until the residual solvent in the nanofiber film was completely removed. Then the films were annealed in a constant temperature oven at 155°C for 4 h. After cooling to room temperature, the PLLA-aligned films were removed from the aluminum foil for the next experiment. The morphology of PLLA films were observed by a SEM, (SU8020, Hitachi, Japan). The crystallization of PLLA thin films were evaluated using a differential scanning calorimeter (Mettler Toledo, Switzerland). XRD and infrared analysis were performed with a PANalytical X'Pert3 diffractometer (the Netherlands) and Vertex 80V infrared spectrometer (Bruker, Germany). Piezoresponse force microscopic (PFM) tests were characterized by an atomic force microscope (AFM, MFP-3D-SA, Asylum Research, USA) with a ferroelectric test system. For the piezoelectric output test under US stimulation, the films were sputtered with gold on both sides and leaded with wires. Then the films were immersed in silicone oil and applied with US. The output performances of PLLA films were measured and recorded by Keithley 6517B electrometer (Tektronix, USA). Static stress-strain curves were tested using a tensile machine (Mark-10). The mechanical properties of PLLA films were tested by dynamic mechanical analysis (DMA, Q800). All tested films were cut into strips of the same size (20 × 5 × 0.2 mm^3). The test temperature was 25°C, the vibration frequency was 5 Hz, and the tensile range was 1%. The BET test was performed by Micromeritics ASAP 2460 from US.

MSC isolation and culture

Rat bone marrow stem cells (rBMSCs) were isolated from the femurs and tibias of neonatal rats (3 days old) (purchased from Beijing Vital River Laboratory Animal Technology) and cultured in α-MEM medium with 1% penicillin-streptomycin and 10% FBS. Cells were maintained in a humidified atmosphere of 5% CO_2 at 37°C, and the culture medium was changed every 2 days. Passages from 2 to 4 were used for the following experiment. The following parameters were used for all ultrasound stimulation groups in the cell experiments: cells were stimulated three times a day using a 1 MHz, 1 W/cm^2 medical ultrasound probe, and each stimulation lasted for 1 min.

Cell compatibility of HAMA

To verify the cell safety of HAMA, cell culture plates and HAMA without UV were used as control groups, and HAMA with UV as experimental group, MSCs were cultured for CCK8 cell viability test on days 1 and 3, and the cell viability was directly proportional to the absorbance of the supernatant at 450 nm in the CCK8 test. In this case, the UV condition was 30 mW/cm^2 power irradiation for 10 s. The cytocompatibility of photocured HAMA was verified to be good (Figure S22).

Construction of the scaffold

First, 1 g of PLLA was dissolved in 10 mL of dichloromethane. After completely dissolved, 2 mL of PEG 200 solution was added into the solution. The mixture was added into a stainless-steel tank, and the solvent was evaporated naturally at room temperature for 24 h. Then the films were washed alternately with deionized water and alcohol three times. The films were wrapped on a stainless-steel column with a diameter of 1 mm and fixed with polytetrafluoroethylene (PTFE) film outside. After insulation at 70°C for 20 min, remove the PTFE film, extract the stainless-steel column, and obtain a cylindrical porous PLLA shell with an inner diameter of approximately 1 mm.

Operated in a biosafety cabinet, rBMSCs were cultured to logarithmic growth stage and seeded on PLLA films. PBS was used to prepare a 2.5% (wt %) HAMA hydrogel solution and fully dissolved in a 37°C water bath. After transferring 50 μL of HAMA hydrogel solution to the surface of the PLLA fiber membrane covered with cells (1 × 1 cm^2) with a pipette, it was immediately irradiated with ultraviolet light for 10 s for photocuring. Before implantation into rats, the scaffolds were immersed in the culture medium environment for the maintenance of the cell viability. The section view of the scaffold was observed by SEM

Please cite this article in press as: Shan et al., A neurodevelopment-inspired self-evolving scaffold for nerve regeneration, Cell Biomaterials (2024), https://doi.org/10.1016/j.celbio.2024.100006

(Nova450, FEI, Czech). The scaffolds were immersed in PBS, SBF and complete medium at 37°C to test their stability. The scaffolds were naturally dried and weighed and photographed at the days 0, 5, 10, and 15, respectively.

Evaluation of MSC differentiation

When rBMSCs were cultured to the logarithmic phase, the cells were seeded on TCPs (round coverslips), PLA-aligned films, and PLLA-aligned films separately. To prevent the material from floating on the bottom of the well plate during the cultivation process, we used custom-made uniform-sized (sterile) polydimethylsiloxane (PDMS) molds to press the materials and circular coverslip onto the bottom of the cell culture well plate to create different cell culture conditions. After 14 days culture and US stimulation, rBMSCs of all the five groups were fixed with 4% PFA for 10 min, permeabilized with 0.5% Triton X-100 for 10 min and blocked in 5% goat serum at room temperature for 40 min. Then, the cells were stained with GFAP and S100 antibody at 4°C overnight. After incubation, the cells were washed with PBS for three times and stained with the secondary antibody (goat anti-rabbit IgG H&L [Alexa Fluor 488] and goat anti-mouse IgG H&L [Alexa Fluor 647]) for 2 h at room temperature. Finally, the cells were stained with DAPI for 10 min and observed with a laser scanning confocal microscope (SP8, Leica, Germany).

In order to quantify the level of cell differentiation, we tested the cells of different groups cultured for 14 days by using qPCR. Total RNA of the cultured cells in different groups were extracted and affinity purified with the FastPure Cell/Tissue Total RNA Isolation Kit. After concentration determination by NanoDrop (Thermo Fisher, USA), total RNA of all the five groups were synthesized into cDNA with approximate concentration. Real-time PCR was performed in triplicate for each sample with real-time fluorescence qPCR instrument (Applied Biosystems StepOnePlus, Thermo Fisher, USA). Gene of GAPDH (served as a housekeeping gene), S100, p75NTR, NGF and NT3 were evaluated (see Table S2 in the supplemental information for primer sequences). The relative transcription levels of target gene expression were normalized to that of GAPDH and expressed as means ± SD (n = 3).

Molecular mechanism *in vitro*

After the attachment of MSC on PLLA-aligned film, the system was assembled and stimulated by US every day for 3 days. D-PBS was used to wash the cells three times, and then a working solution of Fluo 4-AM solution was added to incubate the cells for 30 min at 37°C. D-PBS is a modified buffer that approximates physiological pH and osmotic pressure and helps maintain osmotic pressure balance and pH stability of cells. After removing the Fluo 4-AM solution, the cells were washed with D-PBS again three times and incubated for another 30 min with the D-PBS solution. Images of the cells at the original state were taken using a laser scanning confocal microscope at an excitation wavelength of 494 nm and an emission wavelength of 516 nm. Then the cells were stimulated by ultrasound for 1 min and photographed at the same site immediately.

50 nM of siPiezo1 and siCaV1.2 were transfected into MSCs, respectively, by an electroporator (CUY21EDIT II, BEX, Japan) according to the manufacturer's instructions, then MSCs were cultured on TCPs and PLLA films and stimulated with ultrasound. For western blotting test, the cells were digested and collected in cell lysis buffer with 1 mM phosphatase inhibitors (PMSF) for the extraction of total protein. BCA kit is a protein quantitative kit based on diquinolinic acid (BCA) using colorimetric method to determine total protein concentration and is a commonly used protein measurement method. After splitting on ice for 30 min, the cells were centrifuged for 10 min at 4°C, 12,000 rpm and total protein amount was measured by a BCA kit. Then 5× loading buffer was added, and the samples were boiled for 10 min. Equal amounts of proteins were loaded and fractionated with the 10% SDS-PAGE gels. The gels were run at 80 V for 10 min for the protein concentration and at a constant voltage of 120 V for 1 h for the separation, then wet transfer was performed using PVDF at 250 mA for 2 h. After blocked in 5% skim milk powder solution in tris buffered saline with tween 20 (TBST), membranes were incubated with primary antibodies (Piezo1, $Ca_V1.2$, phosphor-Akt and phospho-p44/42 MAPK [Erk1/2]) overnight at 4°C, respectively. To remove excess primary antibody, the membranes were washed with TBST for three times and then incubated with secondary antibodies for 1.5 h at room temperature. After washing three times, the film was incubated at room temperature in the ECL working liquid for 1 min, and the imprinted film was pasted in the X-ray exposure cassette with plastic wrap, and then the X-ray film was pressed on the film for a few seconds to a few minutes in the darkroom. Protein or nucleic acid bands can be clearly displayed on the X-ray film and exposed by an automatic chemiluminescence image analysis system (Tanon 5200, China).

ELISA was used for the evaluation of the secretion of cell factors. MSC cells of different groups were cultured and stimulated for 14 days, and the cell culture supernatants were collected for the test. ELISA test of β-NGF, VEGF, and BDNF were conducted follow the procedures with ELISA kit.

Transwell assays were performed to valid the effect of promoting migration of this system. PLLA-aligned films were fixed on the bottom of the lower chamber and seeded with rBMSCs. After 3 days of cell culture in the lower chamber and US stimulation, half of the culture medium of the lower chamber was changed, and other rBMSCs were seeded on the upper chamber and cultured for 24 h. Next, the Transwell chambers were fixed with 4% PFA and stained with 0.5% crystal violet for 30 min. The cells not penetrating the filters were swabbed with cotton swabs, and the membrane were observed under a microscope (DMI6000, Leica, Germany).

DRG explant culture and growth assessment

DRGs were obtained from neonatal rats (3 days old). Briefly, the spinal canal was cut along both sides of the dorsal midline of the spine, and after removing the exposed spinal cord, DRG can be seen along both sides of the spine and next to the intervertebral foramen. Then they were carefully extracted and the nerves in the tail were cutoff. For the further culture, DRG explants were seeded on the TCPs (coated with rat tail tendon collagen type I) and PLLA-aligned films (inoculated with rBMSC in advance). After culture and stimulation for 10 days, the explant and the underlying cells were fixed and stained with neuronal marker Tuj1 and astrocyte marker GFAP. The constitutional immunofluorescence

Please cite this article in press as: Shan et al., A neurodevelopment-inspired self-evolving scaffold for nerve regeneration, Cell Biomaterials (2024), https://doi.org/10.1016/j.celbio.2024.100006

photographs were captured by a laser scanning confocal microscope (SP8, Leica, Germany).

Animal experiment

All animal experimental procedures used in the study were performed in compliance with animal welfare ethical regulations and approved by the Experimental Animal Ethics Committee of Beijing Institute of Nanoenergy and Nanosystems (2021003LZ). Female SD rats (200–250 g) were used as the experimental objects, and the animal feeding environment met the requirements of specific pathogen free (SPF). Rats were anesthetized by intraperitoneal injection of pentobarbital sodium (1%, 80 mg/100 g). The rats were fasted for 12 h before operation, and all surgical instruments were autoclaved. The skin was disinfected with iodophor after the hair was removed from the cut on the hind leg of the rat, and the sciatic nerve was exposed after the tissue was separated layer by layer. A dissociation injury was performed in the middle of the nerve, and a gap of 10 mm was formed between the proximal nerve bundle and the distal nerve bundle. In the experimental group, the prepared stent was implanted into the nerve defect site, and the stent and nerve cross-section were carefully sutured with 9-0 surgical suture. In the autogenous nerve transplantation group, the resected nerve was also transplanted back to the original position using 9-0 suture. After implantation, the tissue was reduced layer by layer, and the wound was closed with 5-0 sutures and disinfected with iodor. After the surgery, all the animals were moved to cages and given an intramuscular injection of 1-mL penicillin per day for the next 3 days to prevent infection. All experimental groups that required ultrasound used the same ultrasound stimulation conditions: after the implantation surgery, the experimental animals were stimulated with a medical ultrasonic physiotherapy device once every 2 days after surgery, with a total of 3 min of stimulation divided into three times; each ultrasound was performed for 1 min with an interval of 10 min (1 MHz, 1 W/cm^2). The ultrasound intervention lasted for 1 month.

The rats were anesthetized by intraperitoneal injection of pentobarbital sodium. The sciatic nerves were exposed, and the middle portion of the nerves was removed to create a 10-mm gap between the proximal and distal nerve tracts. For the experimental groups, the prepared scaffolds were transplanted into the defect site of the nerve and sutured with 9-0 sutures. The removed nerves were grafted back using 9-0 sutures for the autograft groups. After the implantation surgery, the wounds were sutured with 5-0 sutures. All the animals were transferred to their cages after surgery. For the animals in the group of US stimulation, they were applied with 1 W/cm^2 of US stimulation for three times every other day.

Stem cell fate tracing

The fate tracing of the implanted MSC cells were evaluated with the EdU detection kit. The incorporation level of EdU-incorporated cells to the number of Hoechst 33342-staining cells was observed by fluorescence staining and quantified by flow cytometry. After labeled with EdU, the EdU$^+$ MSCs were integrated into the scaffolds and implanted into the rats. After 4 weeks implantation, the sciatic nerve tissues were separated, fixed in 4% PFA, dehydrated in gradient alcohols and embedded in paraffin blocks. Then EdU staining was conducted, followed by immunofluorescence staining of Tuj1 and S100 and cell nucleus staining of Hoechst. The immunofluorescence photographs were taken by a confocal microscope (SP8, Leica, Germany).

Histology assessment

Repaired sciatic nerve tissues were dissected from the rats and fixed with 4% PFA. After dehydrated and embedded, histological sections of the longitudinal view and transverse view were prepared. The sections were blocked with 3% bovine serum albumin (BSA) and 10% FBS in 0.3% Triton X-100 for 2 h and stained with the primary antibody of NF200 and S100 overnight at 4°C. Then the sections were incubated with secondary antibody for 2 h at room temperature. The immunofluorescence images of the sections were taken by a panoramic scanner (P250 Flash, 3DHISTECH, Hungary). The images of each group were analyzed by ImageJ for the relative positive area.

For the observation of the ultrastructure of regenerated nerves, pictures were taken with the TEM (Tecnai Spirit 120 kV, FEI, USA). The rats were anesthetized and conducted with cardiac perfusion with 4% PFA and 2.5% glutaraldehyde (GA) solution. Then the fixed tissues were treated with 1% osmium tetroxide for 2 h, dehydrated with graded ethanol and embedded by epoxy resin. The ultrathin sections were processed by the ultramicrotome (EM UC6, Leica, Germany), and the samples were stained by uranyl acetate and lead citrate for the observation under TEM.

Functional recovery analysis

The footprints of the rats in each group at 4, 6, 8, 10, and 12 weeks after implantation were recorded and evaluated into SFI. The rats at 12 weeks after implantation were anesthetized and exposed with sciatic nerves. Then the stimulating electrodes were placed to the nerve trunk proximal to the injury site and the simulation signals were supplied by an electrical nerve stimulation apparatus (Multichannel Systems, Germany). The electrophysiological test was performed, and the CMAP were recorded by Biopac MP150 (USA). Then the bilateral gastrocnemius muscles were separated and weighted. Masson staining of the muscles were conducted and examined with a light microscope (Nikon, Japan).

Transcriptome sequencing and data analysis

After transplantation of the scaffolds for 10 weeks, the sciatic nerves of the rats were removed and immediately frozen in liquid nitrogen. Then total RNA of the tissues were extracted for the sequencing. All the samples were sequenced using the platform at Majorbio (China). For each group, three biological replicates were conducted. The RNA sequencing (RNA-seq) data were analyzed online with the Majorbio platform and the threshold was a fold-change ≥ 2.

Statistical analysis

At least three times of each experiment was conducted independently in this research. Statistical analyses were performed with

CellPress OPEN ACCESS

Cell Biomaterials
Article

GraphPad Prism software and ImageJ software and the results were reported as the mean ± SD. Analysis of significance difference was calculated by using one-way ANOVA with Tukey's multiple comparison test. Statistical differences were shown with four significance levels (*$p < 0.05$, **$p < 0.01$, ***$p < 0.001$, ****$p < 0.0001$).

RESOURCE AVAILABILITY

Lead contact

Further information and requests for resources and reagents should be directed to and will be fulfilled by the lead contact, Zhou Li (zli@binn.cas.cn).

Materials availability

This study did not generate new unique reagents.

Data and code availability

The data supporting the findings in this study are available within the paper and its supplemental information. All data generated in this study are available from the corresponding author on reasonable request. Source data are provided with this paper.

This paper does not report original code

ACKNOWLEDGMENTS

This work was financially supported by the National Key Research and Development Program of China (2022YFB3804700 to Z.L.), National Natural Science Foundation of China (T2125003 and 81971770 to Z.L.; 52372174 to D.L.), Natural Science Foundation of Beijing Municipality (L245015 to Z.L.), Fundamental Research Funds for the Central Universities (EOEG6802X2 and E2E46806 to Z.L.).

AUTHOR CONTRIBUTIONS

Y.S., L.X., and X.C. contributed equally to this work. D.L. and Z.L. were responsible for the experimental concept and design. Y.S., L.X., and X.C. designed the study and performed experimental measurement and data analyses. Y.S. wrote the original manuscript. D.L. and Z.L. reviewed and revised the manuscript. J.Z. and K.R. contributed to the fabrication of piezoelectric films. H.O., J.X., and E.W. contributed to COMSOL simulation. X.W. and J.H. contributed to the validation. D.L. and Z.L. were also responsible for project administration, conceptualization, supervision, and funding acquisition. All authors discussed the results and commented on the manuscript.

DECLARATION OF INTERESTS

The authors declare no competing interests.

SUPPLEMENTAL INFORMATION

Supplemental information can be found online at https://doi.org/10.1016/j.celbio.2024.100006.

Received: August 14, 2024
Revised: November 28, 2024
Accepted: December 11, 2024
Published: January 17, 2025

REFERENCES

1. Scheib, J., and Höke, A. (2013). Advances in peripheral nerve regeneration. Nat. Rev. Neurol. *9*, 668–676. https://doi.org/10.1038/nrneurol.2013.227.
2. Qian, Y., Lin, H., Yan, Z., Shi, J., and Fan, C. (2021). Functional nanomaterials in peripheral nerve regeneration: scaffold design, chemical principles and microenvironmental remodeling. Mater. Today *51*, 165–187. https://doi.org/10.1016/j.mattod.2021.09.014.
3. Avraham, O., Feng, R., Ewan, E.E., Rustenhoven, J., Zhao, G., and Cavalli, V. (2021). Profiling sensory neuron microenvironment after peripheral and central axon injury reveals key pathways for neural repair. eLife *10*, e68457. https://doi.org/10.7554/eLife.68457.
4. Gao, Y., Wang, Y.-L., Kong, D., Qu, B., Su, X.-J., Li, H., and Pi, H.-Y. (2015). Nerve autografts and tissue-engineered materials for the repair of peripheral nerve injuries: a 5-year bibliometric analysis. Neural Regen. Res. *10*, 1003–1008. https://doi.org/10.4103/1673-5374.158369.
5. Hoben, G.M., Ee, X., Schellhardt, L., Yan, Y., Hunter, D.A., Moore, A.M., Snyder-Warwick, A.K., Stewart, S., Mackinnon, S.E., and Wood, M.D. (2018). Increasing nerve autograft length increases senescence and reduces regeneration. Plast. Reconstr. Surg. *142*, 952–961. https://doi.org/10.1097/PRS.0000000000004759.
6. Tian, L., Prabhakaran, M.P., and Ramakrishna, S. (2015). Strategies for regeneration of components of nervous system: scaffolds, cells and biomolecules. Regen. Biomater. *2*, 31–45. https://doi.org/10.1093/rb/rbu017.
7. Lavorato, A., Raimondo, S., Boido, M., Muratori, L., Durante, G., Cofano, F., Vincitorio, F., Petrone, S., Titolo, P., Tartara, F., et al. (2021). Mesenchymal stem cell treatment perspectives in peripheral nerve regeneration: systematic review. Int. J. Mol. Sci. *22*, 572. https://doi.org/10.3390/ijms22020572.
8. Hilton, B.J., Griffin, J.M., Fawcett, J.W., and Bradke, F. (2024). Neuronal maturation and axon regeneration: unfixing circuitry to enable repair. Nat. Rev. Neurosci. *25*, 649–667. https://doi.org/10.1038/s41583-024-00849-3.
9. Goldberg, J.L., and Barres, B.A. (2000). The relationship between neuronal survival and regeneration. Annu. Rev. Neurosci. *23*, 579–612. https://doi.org/10.1146/annurev.neuro.23.1.579.
10. Vijayavenkataraman, S. (2020). Nerve guide conduits for peripheral nerve injury repair: A review on design, materials and fabrication methods. Acta Biomater. *106*, 54–69. https://doi.org/10.1016/j.actbio.2020.02.003.
11. Alasaadi, D.N., Alvizi, L., Hartmann, J., Stillman, N., Moghe, P., Hiiragi, T., and Mayor, R. (2024). Competence for neural crest induction is controlled by hydrostatic pressure through Yap. Nat. Cell Biol. *26*, 530–541. https://doi.org/10.1038/s41556-024-01378-y.
12. Vrij, E.J., Scholte Op Reimer, Y.S., Roa Fuentes, L., Misteli Guerreiro, I., Holzmann, V., Frias Aldeguer, J., Sestini, G., Koo, B.K., Kind, J., van Blitterswijk, C.A., et al. (2022). A pendulum of induction between the epiblast and extra-embryonic endoderm supports post-implantation progression. Development *149*, dev192310. https://doi.org/10.1242/dev.192310.
13. Azagury, M., and Buganim, Y. (2024). Unlocking trophectoderm mysteries: In vivo and in vitro perspectives on human and mouse trophoblast fate induction. Dev. Cell *59*, 941–960. https://doi.org/10.1016/j.devcel.2024.03.029.
14. Jessen, K.R., and Mirsky, R. (2005). The origin and development of glial cells in peripheral nerves. Nat. Rev. Neurosci. *6*, 671–682. https://doi.org/10.1038/nrn1746.
15. Glebova, N.O., and Ginty, D.D. (2005). Growth and survival signals controlling sympathetic nervous system development. Annu. Rev. Neurosci. *28*, 191–222. https://doi.org/10.1146/annurev.neuro.28.061604.135659.
16. Káradóttir, R.T., and Kuo, C.T. (2018). Neuronal activity-dependent control of postnatal neurogenesis and gliogenesis. Annu. Rev. Neurosci. *41*, 139–161. https://doi.org/10.1146/annurev-neuro-072116-031054.
17. Zhang, L.I., and Poo, M.M. (2001). Electrical activity and development of neural circuits. Nat. Neurosci. *4*, 1207–1214. https://doi.org/10.1038/nn753.
18. Tucker, K.L., Meyer, M., and Barde, Y.A. (2001). Neurotrophins are required for nerve growth during development. Nat. Neurosci. *4*, 29–37. https://doi.org/10.1038/82868.
19. Hao, M.M., Lomax, A.E., McKeown, S.J., Reid, C.A., Young, H.M., and Bornstein, J.C. (2012). Early development of electrical excitability in the

mouse enteric nervous system. J. Neurosci. *32*, 10949–10960. https://doi.org/10.1523/JNEUROSCI.1426-12.2012.

20. Levin, M., Pezzulo, G., and Finkelstein, J.M. (2017). Endogenous bioelectric signaling networks: exploiting voltage gradients for control of growth and form. Annu. Rev. Biomed. Eng. *19*, 353–387. https://doi.org/10.1146/annurev-bioeng-071114-040647.
21. Nuccitelli, R. (2003). Endogenous electric fields in embryos during development, regeneration and wound healing. Radiat. Prot. Dosimetry *106*, 375–383. https://doi.org/10.1093/oxfordjournals.rpd.a006375.
22. Arulkandarajah, K.H., Osterstock, G., Lafont, A., Le Corronc, H., Escalas, N., Corsini, S., Le Bras, B., Chenane, L., Boeri, J., Czarnecki, A., et al. (2021). Neuroepithelial progenitors generate and propagate non-neuronal action potentials across the spinal cord. Curr. Biol. *31*, 4584–4595.e4. https://doi.org/10.1016/j.cub.2021.08.019.
23. Spitzer, N.C. (2006). Electrical activity in early neuronal development. Nature *444*, 707–712. https://doi.org/10.1038/nature05300.
24. Cafarelli, A., Marino, A., Vannozzi, L., Puigmartí-Luis, J., Pané, S., Ciofani, G., and Ricotti, L. (2021). Piezoelectric nanomaterials activated by ultrasound: the pathway from discovery to future clinical adoption. ACS Nano *15*, 11066–11086. https://doi.org/10.1021/acsnano.1c03087.
25. Curry, E.J., Ke, K., Chorsi, M.T., Wrobel, K.S., Miller, A.N., Patel, A., Kim, I., Feng, J., Yue, L., Wu, Q., et al. (2018). Biodegradable piezoelectric force sensor. Proc. Natl. Acad. Sci. USA *115*, 909–914. https://doi.org/10.1073/pnas.1710874115.
26. Curry, E.J., Le, T.T., Das, R., Ke, K., Santorella, E.M., Paul, D., Chorsi, M.T., Tran, K.T.M., Baroody, J., Borges, E.R., et al. (2020). Biodegradable nanofiber-based piezoelectric transducer. Proc. Natl. Acad. Sci. USA *117*, 214–220. https://doi.org/10.1073/pnas.1910343117.
27. Farahani, A., Zarei-Hanzaki, A., Abedi, H.R., Tayebi, L., and Mostafavi, E. (2021). Polylactic acid piezo-biopolymers: chemistry, structural evolution, fabrication methods, and tissue engineering applications. J. Funct. Biomater. *12*, 71. https://doi.org/10.3390/jfb12040071.
28. Tai, Y., Yang, S., Yu, S., Banerjee, A., Myung, N.V., and Nam, J. (2021). Modulation of piezoelectric properties in electrospun PLLA nanofibers for application-specific self-powered stem cell culture platforms. Nano Energy *89*, 106444. https://doi.org/10.1016/j.nanoen.2021.106444.
29. Pan, P., Zhu, B., Kai, W., Dong, T., and Inoue, Y. (2008). Polymorphic transition in disordered poly(l-lactide) crystals induced by annealing at elevated temperatures. Macromolecules *41*, 4296–4304. https://doi.org/10.1021/ma800343g.
30. Mano, J.F., Gómez Ribelles, J.L., Alves, N.M., and Salmerón Sanchez, M. (2005). Glass transition dynamics and structural relaxation of PLLA studied by DSC: Influence of crystallinity. Polymer *46*, 8258–8265. https://doi.org/10.1016/j.polymer.2005.06.096.
31. Chorsi, M.T., Curry, E.J., Chorsi, H.T., Das, R., Baroody, J., Purohit, P.K., Ilies, H., and Nguyen, T.D. (2019). Piezoelectric biomaterials for sensors and actuators. Adv. Mater. *31*, e1802084. https://doi.org/10.1002/adma.201802084.
32. Yousry, Y.M., Wong, V.-K., Ji, R., Chen, Y., Chen, S., Zhang, X., Lim, D.B.K., Shen, L., and Yao, K. (2023). Shear mode ultrasonic transducers from flexible piezoelectric PLLA fibers for structural health monitoring. Adv. Funct. Mater. *33*, 2213582. https://doi.org/10.1002/adfm.202213582.
33. Yan, X., Liu, J., Ye, Z., Huang, J., He, F., Xiao, W., Hu, X., and Luo, Z. (2016). CaMKII-mediated CREB phosphorylation is involved in Ca^{2+}-induced BDNF mRNA transcription and neurite outgrowth promoted by electrical stimulation. PLoS One *11*, e0162784. https://doi.org/10.1371/journal.pone.0162784.
34. Ureshino, R.P., Erustes, A.G., Bassani, T.B., Wachilewski, P., Guarache, G.C., Nascimento, A.C., Costa, A.J., Smaili, S.S., and Pereira, G.J.D.S. (2019). The interplay between Ca^{2+} signaling pathways and neurodegeneration. Int. J. Mol. Sci. *20*, 6004. https://doi.org/10.3390/ijms20236004.
35. Wenjin, W., Wenchao, L., Hao, Z., Feng, L., Yan, W., Wodong, S., Xianqun, F., and Wenlong, D. (2011). Electrical stimulation promotes bdnf expression in spinal cord neurons through Ca^{2+} and ERK-dependent signaling pathways. Cell. Mol. Neurobiol. *31*, 459–467. https://doi.org/10.1007/s10571-010-9639-0.
36. Peng, B., Rao, Y., Wang, Y., Duan, S., Qi, H., Yang, J., and Zhang, H. (2024). Immunology reshapes neuroscience, and neuroscience reshapes immunology. Fundam. Res. *4*, 199–200. https://doi.org/10.1016/j.fmre.2024.01.003.